New evidence of Proterozoic high P-T metamorphism in East Antarctica from thermobarometry and *in-situ* U-Pb age dating of monazite in metamorphic glacial clasts, central Transantarctic Mountains, Antarctica

SUBMITTED TO THE FACULTY OF THE

UNIVERSITY OF MINNESOTA-DULUTH

BY

CHELSEA I. NISSEN

IN PARTIAL FULFILLMENT OF THE REQUIREMENTS

FOR THE DEGREE OF

MASTER OF SCIENCE

DR. JOHN GOODGE

NOVEMBER 2014

The important thing is to never stop questioning. Curiosity has its own reason for existing.

-Albert Einstein

Acknowledgements

First and foremost, I want to extend a very huge thanks to my advisor, Dr. John Goodge. His relentless patience and support over the last two years has been nothing but incredible, especially during this past very long and busy year. I would not have been able to accomplish even half of what I've done without such amazing feedback and encouragement. Thank you.

Thanks to my committee members, Dr. Paul Siders and Dr. Vicki Hansen. Both have been extremely flexible and supportive of this work. Their positive feedback, suggestions and support are enormously appreciated. Thank you to Mark Fanning, at ANU, for offering guidance and assistance during long hours and late nights using the SHRIMP, as well as being a friendly support in edits and feedback for presentations and writing. Thank you, Bin Fu, for sample preparation and organization. I would also like to thank Bryan Bandli. He's been a great teacher and provided great help finding tiny little monazites on the SEM. Thank you to Anette von der Handt for all of her generous assistance and patience during data collection and the numerous questions.

I'm grateful to the NSF for their financial support to make this research possible. I am also indebted to the Graduate School, Department of Geology, and Swenson School of Science and Engineering for sponsoring me over the summers and for travel funds to GSA and Australia.

Thank you, Emily Walsh for inspiring my passion for metamorphic petrology and encouraging me to pursue graduate school. Looking back, I can't believe the patience you had with my first attempts at writing and research. Thank you. Robin, thank you for enduring countless edits, phone calls, and overall panic as I worked on my thesis. You are truly one-of-a-kind and I can only hope to reciprocate the favor one day. Seth, a special thanks to you for your continuous support and patience.

Abstract

The East Antarctic shield (EAS) is a key component in the study of early crustal evolution due to its ancient geologic history and involvement in the amalgamation and break-up of major supercontinents. The EAS has documented affinities with the cratons of Africa, India, and Australia based on limited coastal outcrop, but an ice cap up to 4 km thick prevents direct access to the interior bedrock of the EAS. Additionally, thermomechanical effects of the Ross Orogeny (~500 Ma) obscure the Precambrian history in rarely-exposed crystalline basement. Metamorphic rock clasts from glacial moraines near the central Transantarctic Mountains were studied for petrologic, geochemical, and isotopic characteristics in order to further understand the geologic history of the EAS. These clasts were presumably eroded from the interior of the EAS and may provide unique natural samples of the ice-covered basement. Metamorphic rock clasts selected in this study are semi-pelitic gneisses with high-pressure mineral assemblages, as well as accessory minerals including monazite and zircon. New *in-situ* SHRIMP U-Pb analysis of monazite yielded Paleoproterozoic to Neoproterozoic ages in six clasts. Among these, two clasts from Lonewolf Nunataks, at the head of Byrd Glacier, gave previously unrecognized ages of ~1900-1700 Ma, with one having a Mesoproterozoic overprint at ~1200 Ma. Lonewolf Nunataks clasts preserve evidence of high-pressure granulite-facies metamorphic conditions associated with Proterozoic crustal convergence and thickening during orogenic activity. Clasts sampled from moraines near the Miller Range yielded Neoproterozoic U-Pb ages; one clast yielded ages of ~660 and

~590 Ma, whereas other clasts gave ages of ~570- 545 Ma. Neoproterozoic samples conducive to thermobarometric analysis record high P-T conditions comparable to previously documented Ross Orogen activity in reactivated Precambrian crystalline rocks of the Nimrod Group. Together, the clast ages coupled with P-T analysis record previously unknown Paleoproterozoic tectonometamorphic events in central East Antarctica, overprinted by younger Mesoproterozoic metamorphism. Clasts from Lonewolf Nunataks may reflect a Paleoproterozoic event within the EAS related to development of the Nuna supercontinent (~1870-1900 Ma), overprinted by a Mesoproterozoic orogenic event, possibly related to the final amalgamation of Rodinia (~1200 Ma). One clast with a metamorphic age of ~660 Ma may record rift-margin activity associated with supercontinent breakup. Neoproterozoic ages of ~590-545 Ma from some of the clasts are demonstrably older than Ross Orogen ages known from Nimrod Group metamorphic basement; these older ages may therefore provide evidence that Ross orogenic activity was initiated earlier than previously thought, and that its metamorphic overprint extends farther inboard of the Transantarctic Mountains.

Table of Contents

List of Figures

List of Tables

Introduction

The East Antarctic shield (EAS) is a key element in the study of early crustal evolution due to its ancient geologic history and long-lived involvement in the amalgamation and break-up of major supercontinents, notably Nuna, Rodinia and Gondwana (Boger, 2011; Harley & Kelly, 2007). The EAS has geological and chronological affinities with cratons in Africa, India, and Australia, but layers of ice, up to 4 kilometers thick, prevent direct geological access to most of the EAS (Fig. 1). Additionally, much of the Precambrian history of the EAS is obscured as a result of the Ross and Pan-African Orogenies (~650-500 Ma) that resulted in regional deformation, high-grade metamorphism and thermal re-equilibration of crystalline basement (Goodge et al., 2007).

We can use the ice to our advantage by studying glacially transported rock clasts. Geographically and tectonically, the Transantarctic Mountains (TAM) separate the EAS from the younger West Antarctic geologic province (Fig. 1A), yet outlet glaciers that cross the TAM serve to channel ice toward the Ross Ice Shelf from catchment areas in central East Antarctica. Glacial clasts deposited in moraines and tills along the inboard edge of the TAM are likely eroded from a cratonic source within catchment areas >1000 km inboard (Rignot et al., 2011). We can assume that these clasts originated in the central EAS based on known ice-flow directions, aeromagnetic signatures from ice-covered basement, and depositional location relative to ice catchment basins (Fig. 1; Goodge et al., 2010; Goodge and Finn, 2010). Thus, glaciogenic material may be used as natural proxy samples of the ice-covered basement of East Antarctica.

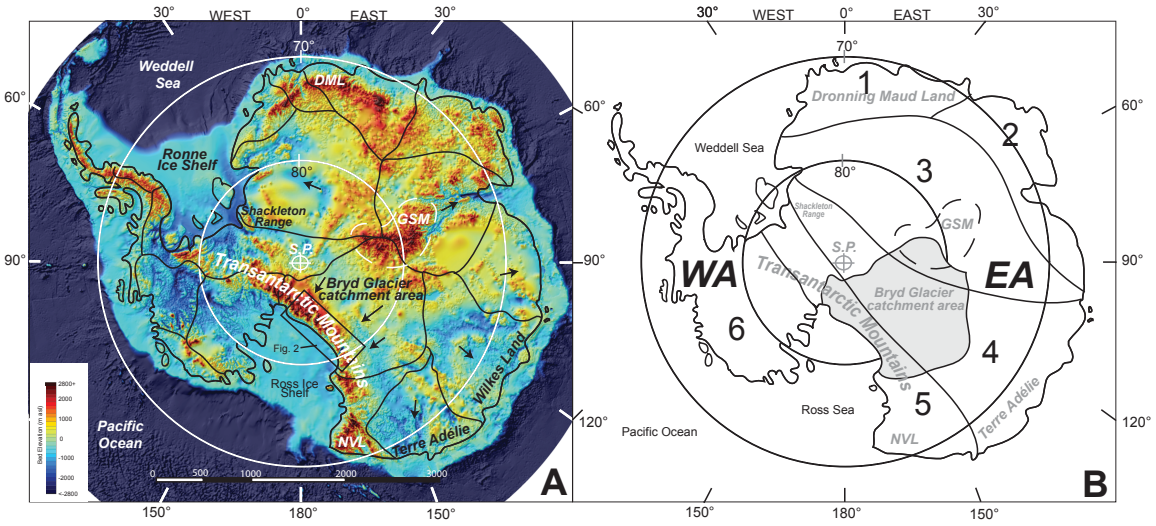

Figure 1: A) BEDMAP image of Antarctica showing major geographic features. Black lines represent major ice catchment divides (Rignot et al., 2011) and arrows indicate general ice-flow directions. White dashed-line represents general location of the Gamburtsev Subglacial Mountains (GSM). Box indicates area of Figure 2. **B)** General map of Antarctica showing major known crustal affinities. 1= African affinities; 2= Indian affinities; 3= Unknown crustal affinities 4= Australian affinities; 5= Ross orogenic belt; 6=Post-Gondwana accretionary / West Antarctica province. WA= West Antarctica; EA=East Antarctica. Modified from Boger (2011).

Igneous and metamorphic rock clasts were collected from glacial moraines at 12 sample sites along the TAM during the 2010-2011 austral summer. The geographic and lithologic diversity of these clasts can be filtered with petrologic, geochemical and isotopic techniques in order to establish the presence of previously unknown geohistories in the central EAS. For the purposes of this study, we focused on seven high-grade gneissic clasts collected from moraines near the inlet to Byrd Glacier and adjacent to the Miller Range (Fig. 2). A comparison of metamorphic histories recorded in the glacial clasts and in basement exposures in the TAM will further our understanding of the crustal and tectonic history of the central EAS.

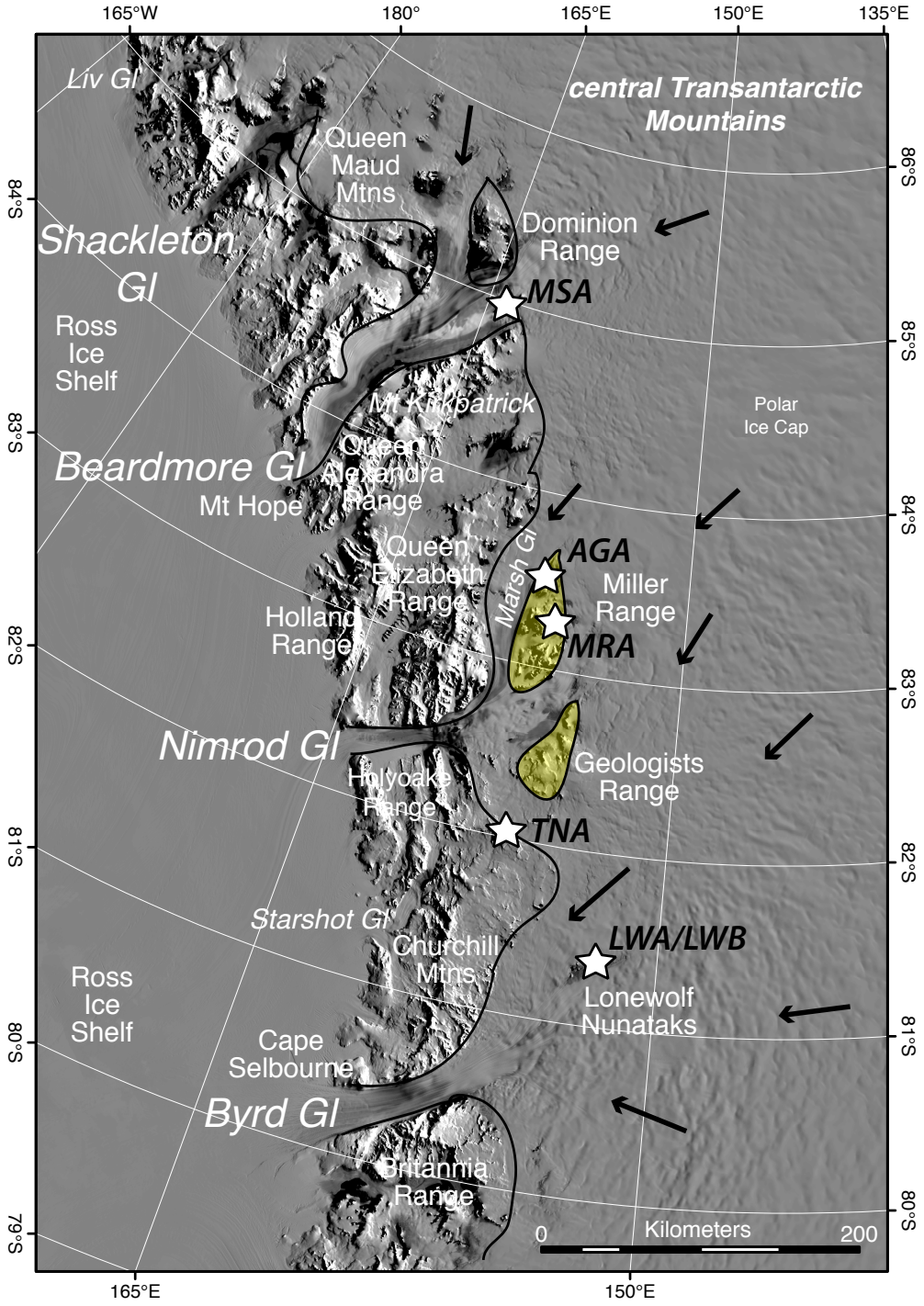

Figure 2: Moderate resolution imaging spectroradiometer (MODIS) satellite image of the central TAM area, showing major geographic features. Stars indicate sample locations. This study focuses on metamorphic glacial clast samples collected from Argo Glacier (AGA) and Milan Ridge (MRA) sites near the Miller Range and Lonewolf Nuntaks site B (LWB). Other sample sites include Mount Sirius (MSA), Turret Nunatak (TNA) and Lonewolf Nunataks site A (LWA). Arrows indicate predicted ice-flow directions and black lines indicate approximate outcrop boundaries. Shaded yellow region shows known Precambrian bedrock exposure. Modified from Goodge (manuscript in review).

In order to elucidate the metamorphic history of clasts derived from the central EAS,for each clast we sought to constrain mineral parageneses, pressure-temperature (P-T) conditions of formation, and age of formation by monazite U-Pb geochronology. We focused on clasts with ages >500 Ma, in order to avoid the extent of possible effects of the Ross Orogen. For these metamorphic rocks, a combination of monazite ages coupled with their textural setting and P-T estimates help to reconstruct the crustal conditions and pressure-temperature-time evolution. Clasts from this study record a previously unknown metamorphic event in central EAS of ~1900 Ma, overprinted by a ~1200 Ma event that corresponds to recently identified magmatic ages (Goodge et al., 2010, 2012). These samples may record a significant metamorphic event within the EAS related to the assembly of the Nuna supercontinent (~1870-1900 Ma), later affected by Grenvillian events related to Rodinia amalgamation. Clasts also record ages of ~650-550 Ma that may signal earlier tectonic activity associated with the Ross Orogeny than previously thought.

Geologic Background

Precambrian rocks of the EAS are exposed along the Antarctic coast and in the central TAM. Previous studies from the TAM sector reveal several distinct age domains at ~3.1, ~2.5, ~1.7, ~1.4 and ~1.1 Ga, indicating the presence of a large composite crustal province beneath the ice (Peucat et al., 1999; Goodge and Fanning, 1999; Goodge et al., 2001; Goodge et al., 2008; Fitzsimons et al., 2000; Fitzsimons et al., 2003; Boger, 2011).

A single crustal unit, previously defined as the Mawson Continent and herein referred to as the Mawson craton, is thought to comprise the core of the central EAS and has associations with the Gawler craton in Australia (Fanning and Oliver, 1995; Boger et al., 2011). Due to ice cover, the inland extent of this crustal block in the EAS is unknown. Rocks associated with the Mawson craton in the TAM are exposed discontinuously from Terre Adélie to the Nimrod Glacier area and the Shackleton Range (Peucat 1999; Goodge et al., 2001; Fitzsimons, 2003; Zeh; 2004; Harley & Kelly, 2007; Boger, 2011). The Mawson craton includes some of the oldest rocks in Antarctica with ages up to 3.1 Ga and tectonothermal events at ~2.5, ~1.7, ~1.6, ~1.3 and ~1.1 Ga (Oliver and Fanning, 2002; Fanning et al., 1995 Goodge, et al., 2001; Boger, 2011). Initial growth of the Mawson craton between ~3.0-2.5 Ga is recorded by inherited zircon ages in gneisses, granitoids, and metasediments from Antarctica and Australia (Monnier, 1995; Peucat, 1999; Goodge and Fanning, 1999; Payne et al., 2009; Boger, 2011). Nimrod-Kimban orogenic events (~1.7-1.6 Ga) modified Archean crust of the Mawson craton, as recorded by tectonothermal events in both Australian and Antarctic crust (Goodge et al., 2001; Payne et al., 2009). The Nimrod Orogeny is thought to have formed by arc-continent or continent-continent convergence, which may be related to the fundamental petrotectonic assembly of the Mawson craton (Goodge et al., 2001).

Supercontinent history

Precambrian ages from the EAS correlate globally with the development of other ancient landmasses, including parts of the African, Indian and Australian cratons (Fig. 1B). These connections may signify the EAS as a major component in supercontinent evolution. Due to a lack of paleomagnetic data, the position of the EAS in supercontinent reconstructions is speculative for Nuna and Rodinia.

The evolution of the Nuna supercontinent remains conjectural and Nuna reconstructions often disregard the EAS. Nuna started forming at ~1900 Ma and is thought to be coherent until approximately 1300 Ma (Rogers and Santosh, 2002; Zhao et al., 2002; Evans and Mitchell, 2011). Several hypotheses propose the continuity of Paleoproterozoic fold belts extending from the Nuna cratons into the EAS, but the geologic basis for these ideas is fragmentary (Payne et al., 2009; Zhang et al., 2012, Pisarevsky et al., 2014).

The EAS played a key role in the assembly of the supercontinent Rodinia, which formed between ~1300-900 Ma. The Laurentian craton (present-day Greenland and North America) is central to most Rodinia reconstructions, but the geometry and timing of its western, eastern and northern neighbors remains highly controversial. Likewise, many paleogeographic models of Rodinia include the Mawson craton as a central element. Some models (i.e. SWEAT; Moores, 1991; Hoffman, 1991; Borg and DePaolo 1994; Goodge et al., 2008) offer geological plausibility of a connection between western Laurentia and a linked Australia-East Antarctica craton as recently as ~700 Ma, yet they appear at odds with some paleomagnetic data (e.g., Li et al., 2008; Pisarevsky et al., 2014). The

possibility of a direct crustal link between Laurentia and the Mawson craton at the time of Rodinia amalgamation (~1.1-1.0 Ga) may be addressed by developing a clearer understanding of East Antarctic geology along the TAM sector.

Parts of cratonic Africa and India were contiguous with the EAS during the formation of East Gondwana. The East African Orogen (~650 Ma) defines the boundary between the EAS and African cratons. Later, the Kuunga Orogeny (~550 Ma) formed the boundary between the Indian shield and EAS (Boger, 2011). These Neoproterozoic collisional events (Kuunga and East African orogens) connected the EAS to African and Indian cratons during the formation of Gondwana, yet the continuity of these orogenic belts through central East Antarctica remains highly conjectural (Fig. 1B; Boger, 2011).

The Neoproterozoic-Cambrian Ross Orogeny, also associated with the amalgamation of Gondwana between ~550-480 Ma, overprints older events and signatures along the broadly- defined Tasmanide margin (Cawood et al., 2009; Goodge, 2007). This Andean-style orogeny affected basement rocks of the present-day TAM, such that many primary features of the Precambrian crust have been lost due to basement reactivation by deformation and high-grade metamorphism. However, pre-Ross events are recognized through the dating of monazites and zircons in glacial clasts that appear to have been eroded from the deeper Antarctic interior.

Gamburtsev Subglacial Mountains

The Gamburtstev Subglacial Mountains are located beneath the ice in central East Antarctica (Fig. 1); however, the formation and evolution of these intra-plate mountains remains enigmatic. Based on seismological data, they exhibit a thick, crustal root (>40 km) that is interpreted to be Precambrian in age (Ferraccioli et al., 2011). This crust has anomalously high densities, similar to modeled collisional orogens. Based on the dense crustal root of these mountains, as well as surrounding Paleoproterozoic and Meso- to Neoproterozoic detrital zircon ages from ice cores, it appears that these mountains are related to a Proterozoic continental collisional event, possibly associated with Rodinia or earlier supercontinent assembly (Ferraccioli et al., 2011). There is potential for the analysis of glacial clasts to provide information about the Gamburtsev Mountains given that their western flank lies within the Byrd Glacier catchment (Fig. 1).

Evidence of Precambrian Basement in central East Antarctica

The Precambrian history of the EAS to date has been pieced together by study of bedrock exposure, aeromagnetic imaging, and analysis of glacial clasts. Each method provides unique insight into the interior of the continent, but they also have certain limitations. Exposed bedrock is scarce and commonly overprinted by younger events, such as the Pan-African and Ross orogenies (~650-500 Ma). Aeromagnetic surveys image several hundred kilometers inland, but lack any direct rock observation and sampling. Glacial rock clasts can be

transported from >1000 km inland, depending the size of the catchment area, and provide direct rock observations, however more specific location of each clast source is unknown. Thus, complementary combination of all of these methods collectively reveals aspects of the geological history of the EAS. This study focuses of metamorphic glacial clasts to investigate Precambrian events previously unrecorded the cental EAS.

Exposed Bedrock

The basement geology of the TAM provides some clues to the continental interior. Exposed Precambrian crust in the TAM, adjacent to central East Antarctica, is limited to the Nimrod Group of the Miller and Geologists ranges (Fig. 2). The Nimrod Group is an assemblage of moderate to high-grade rocks with igneous and sedimentary protoliths, including layered gneisses and orthogneisses, schists, quartzites, amphibolites, migmatites, marbles and eclogites (Grindley et al., 1964; Goodge et al., 1993; Peacock and Goodge, 1995). Rocks belonging to the Nimrod Group record several episodes of tectonic activity beginning in the Archean, shown by U-Pb zircon ages of ~3100-3000 Ma (Bennett and Fanning, 1993; Goodge & Fanning, 1999). Zircons in these gneisses reveal growth patterns indicating formation of an Archean igneous protolith of ~3.1 Ga, followed by high-temperature metamorphism at ~2.9 Ga (Goodge and Fanning, 1999). Rocks were further modified during the Nimrod Orogeny at ~ 1.7 Ga, characterized by deep-crustal metamorphism, orogenesis, and magmatism. This orogenic event resulted in high-grade eclogite-facies

metamorphism signifying crustal thickening and possible collision (Peacock and Goodge, 1995; Goodge et al., 2001). The Ross Orogeny triggered basement reactivation at ~550 Ma and resulted in a high-grade dynamothermal metamorphic overprint on the Nimrod Group gneisses, making it difficult to fully resolve the Precambrian history of this section of the EAS (Goodge et al., 1992, 1993).

Included in the greater TAM sector are rock exposures in Terre Adélie and Wilkes Land to the north and the Shackleton Range to the south. Archean rocks (~2.8-2.4 Ga) with a Paleoproterozoic overprint (~1.7 Ga) are found in Terre Adélie (Peucat et al., 1999). These high-grade metaigneous and gneissic rocks are correlated with the Archean-Proterozoic Gawler craton in Australia and support a hypothesis of one continuous crustal province, the Mawson craton (Oliver and Fanning, 1995; Boger, 2011). Distinctive felsic volcanic rocks with an age of ~1.6 Ga in glacial moraines of Terre Adélie confirm the presence of Precambrian basement, like that in the Gawler craton, underlying this sector of the East Antarctic ice sheet. Glaciomarine rock clasts collected from offshore Wilkes Land yielded a dominant metamorphic and igneous zircon age component of ~500 Ma with evidence of ~670-780, 900-1300, 1740-2300 and >2700 Ma inherited events (Goodge and Fanning, 2010). This study also reported detrital zircon ages from glaciomarine sediments that support an inland source of Neoproterozoic, Paleoproterozoic and Archean basement underneath the ice.

South of the TAM, rocks of similarly distinct Archean and Paleoporterozoic age occur in the Shackleton Range (Harley et al., 2007; Will et al., 2010). These moderate- to high-grade gneisses yield detrital zircon ages of ~2.8-2.4 Ga, as well primary igneous ages of ~2.1-2.0 Ga, with emplacement at 1.8 Ga and high-T granulite-facies metamorphism at ~1.7 Ga (Will et al., 2010). These age data are consistent with those from the Mawson craton elsewhere in Antarctica (i.e. Nimrod Group and Terre Adélie) as well as the Gawler Craton proper (Peucat et al., 1999; Fanning et al., 2007; Goodge et al., 2001). Pan-African orogenic events (~650 Ma) overprint rocks in the Shackleton Range and obscure the Precambrian history (Harley et al, 2007).

Magnetic Anomaly Mapping

Aeromagnetic imaging in transects across the TAM and over the East Antarctic ice sheet reveals magnetic intensity variations and the structure of underlying Precambrian crust (Ferraccioli et al. 2009; Goodge and Finn, 2010; Ferraccioli et al., 2011; Jordan et al., 2013). In the central TAM, Goodge and Finn (2010) conducted an aeromagnetic survey comparing exposed basement rocks of the Nimrod Group to the inland ice-covered basement. They interpreted subglacial anomalies as the signature of Archean basement intruded by Proterozoic magmatism. In addition, km-scale basement fabrics associated with the Ross Orogen extend farther inland (~100 km) than previously thought. Igneous clast ages of ~1.8-1.1 Ga from moraines at Lonewolf Nunataks and near the Miller Range may serve as samples of these aeromagnetic anomalies, and

indicate the presence of Proterozoic crust not observed in outcrop (Goodge et al., 2008, 2010).

To the north in the Wilkes subglacial basin, an aeromagnetic anomaly defines the boundary between Proterozoic units of the Mawson craton and Ross orogenic rocks (Goodge and Finn, 2010; Jordan et al., 2013). These studies support previous work by Ferraccioli et al. (2009), who observed a distinction between the Wilkes basin and Precambrian crust to the west. Corridor aeromagnetic and satellite magnetic data, combined with seismic velocity data, clearly indicate the presence of 35-40 km-thick crust beneath much of East Antarctica (Lawrence et al., 2006).

Aeromagnetic imaging over the Gamburtsev Subglacial Mountain region is interpreted to reveal thick crustal roots with large-scale structures separating distinct blocks (Ferraccioli et al., 2011). Ferraccioli et al. (2011) reinforced the idea of a composite craton formed during Proterozoic orogenic events beneath the EAS. The magnetic anomalies that typify the Gamburtsev Subglacial Mountains are similar to Precambrian signatures of granites and othogneisses to the north.

Ice Flow and Glacial Clast Transport

Glacial rock clasts transported from the interior of the EAS can help clarify the Precambrian history through direct rock sampling. Ice from the East Antarctic ice sheet spreads laterally in discrete catchments and is funneled through outlet glaciers that traverse the TAM and drain into the Ross Ice Shelf (Figs. 1A and 2).

The largest of these glacial drainages feeds the Byrd Glacier. Ice is transported from more than 1000 km inland and moves at varying rates from ~1.5 m/year up to ~800 m/year through the Byrd Glacier (Stearns et al., 2008; Rignot et al., 2011). Although the physical conditions at its base are poorly known, the massive East Antarctic ice sheet has the ability to erode underlying bedrock and transport rock debris laterally though glacier drainages. Ablation of ice as it ramps up against the inland side of the mountain range exposes glacial lags and coherent moraines. Glacial rock clasts collected in moraines at the margin of the TAM may therefore have been transported from central regions of the EAS, by a mechanism similar to the glacial transport of entrained meteorites (Whillans and Cassidy, 1983).

Glacial rock clasts for this study were collected from three moraines: at Milan Ridge and Argo Glacier, both near Nimrod Glacier and adjacent to the Miller Range, and Lonewolf Nunataks, near Byrd Glacier (Fig. 2). From a large, diverse collection of igneous and metamorphic rock clasts, this study focused on high-grade pelitic to semi-pelitic gneisses from which both P-T and age information could be obtained. As shown in previous studies (Goodge et al., 2008, 2010), glacial-clast analysis can lead to a more robust understanding of the ice-covered bedrock in central East Antarctica.

Methods

Seven samples were selected for detailed study based on geographic location, mineral assemblage, metamorphic textures, and abundance and size of

monazite grains. Initial screening of metamorphic clasts was undertaken to identify mineral assemblages conducive to P-T study and monazite for geochronology. Previous petrographic study of clasts that met these criteria (Radakovich, 2013) was helpful in narrowing the selected candidates to the Lonewolf Nunataks (LWB) and Miller Range (Argo Glacier and Milan Ridge; AGA and MRA respectively) sample sites. Clasts from LWB are potentially important as representatives of the EAS due to their inland provenance inferred from the large catchment area of the Byrd Glacier, demonstrated by the finding of Proterozoic igneous clasts (Goodge et al., 2012). Clasts from AGA and MRA were chosen because previously discovered Precambrian igneous clasts contrast in age with the known history of the Nimrod Group (Goodge et al., 2008, 2010).

Minerals and petrologic textures were studied using a petrographic microscope in order to identify samples containing minerals suitable for P-T analysis (i.e., garnet and Al-silicate), U-Pb radiometric dating (i.e., monazite), and grain textures indicating thermodynamic equilibrium (i.e., well-defined grain shapes and grain boundaries, and absence of reaction textures). The seven samples in this study each have a mineral assemblage containing garnet, feldspars, Al-silicate, micas, and monazite. Samples were analyzed at the University of Minnesota-Duluth on a JEOL JSM-6490LV scanning electron microscope to confirm metamorphic assemblages and locations of monazite. Electron backscatter images show that most monazite grains are compositional zoned.

Monazite U-Pb ages were determined for all seven samples using a sensitive high-resolution ion microprobe (SHRIMP). Monazites were analyzed *in-situ* using a SHRIMP II at the Australian National University under standard operating conditions with a spot size of 10 μm. Monazite grains range in size from 15-50 μm. Selected areas of ~2-3 mm diameter were cut from polished thin sections using an ultrasonic drill and mounted in a polished epoxy megamount of 35 mm diameter. Monazite spots from the clast samples were analyzed along with monazite reference standard 44069.

Of the seven samples, four were analyzed further by electron probe microanalyzer (EPMA) to determine chemical compositions of minerals to be used for P-T estimates. Samples were analyzed using a JEOL JXA-8900 electron microprobe at the University of Minnesota-Twin Cities with an accelerating voltage of 15 kV and a beam current of 20 nA. A beam diameter of 1 μm was used for garnet and feldspar, and a 5 μm-diameter beam was used for biotite. P-T conditions were modeled using mineral compositions as an input for the thermodynamic modeling program THERMOCALC (Powell & Holland, 1988, 1994).

Results

Petrography

Clast 10AGA-7.4

Clast 10AGA-7.4, a well-foliated garnet-biotite-sillimanite paragneiss, displays 1-2 centimeter garnet-biotite-oxide bands alternating with quartz-

plagioclase layers (Figure 3). This clast is composed of quartz, plagioclase, alkali feldspar, garnet, biotite, and sillimanite, with accessory apatite, rutile, monazite and zircon (Figure 4). Quartz occurs as inclusions in garnet and as ribbons in the matrix with undulose extinction. Feldspars occur as inclusions in garnet and in the matrix. Plagioclase (An_{39}) is optically and compositionally homogenous. Plagioclase and alkali feldspar (Or_{95}) grains exhibit myrmekite textures.

Garnets, which range in size from a few millimeters to one centimeter, are hypidioblastic with inclusions of mica, plagioclase, quartz and apatite. Two garnets (B and D) were analyzed on the EPMA for compositional variation. A line traverse across both garnets shows that they are almandine-rich with significant compositional variation ($Alm_{47-63}Pyp_{10-33}Grs_{5-30}Sps_{<1}$; Fig.5). The spessartine (Mn) component in both garnets is negligible with respect to other end-member components (Alm, Pyp, Grs) and therefore excluded from Figure 5. Prograde metamorphic signatures in this sample include increasing pyrope component with decreasing almandine from core to rim of the garnet. The grossular component is uniform across transects, with a decrease at the rim.

Biotite, which occurs mostly along the edges of garnet grains or within the foliation near the garnets, is light brown to rust color. Biotite shows little compositional variation with an average Mg/(Mg+Fe) ratio of 0.66. Kyanite and sillimanite are present in the sample. In places, kyanite grains are elongate to prismatic (following foliation) with fibrous sillimanite radiating outwards from kyanite edges. Small clusters of late radial fibrolitic sillimanite crosscut neighboring minerals and appear to be post-kinematic.

Apatite and rutile occur as inclusions in garnet. Rutile also occurs in the matrix along the foliations. Monazite and zircon occur mostly as inclusions in other phases, although zircon grains also occur within the matrix. Monazite is 10-100 microns in size and shows patchy zoning in backscattered images (Fig. 6).

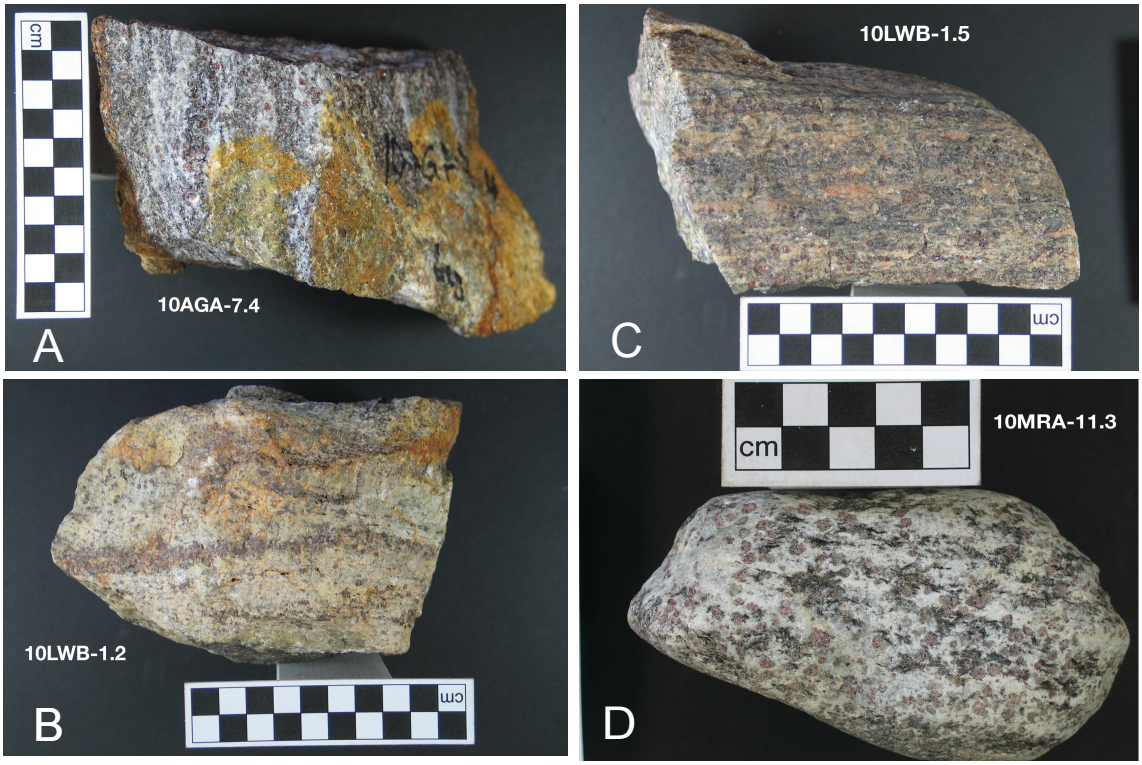

Figure 3: Photographs of metamorphic glacial clasts. A) 10AGA-7.4, Grt-Bt-Silparagneiss; B) 10LWB-1.2, Grt-Bt-Ky gneiss; C) 10LWB-1.5, Grt-Bt-Ms gneiss; D) 10MRA-11.3, Grt-Bt gneiss.

Clast 10LWB-1.2

Clast 10LWB-1.2, a well-foliated leucocratic garnet-biotite-kyanite gneiss, displays cream-colored bands alternating with darker layers of garnet and oxides (Figure 3). It is composed of quartz, plagioclase, alkali feldspar, garnet, biotite and kyanite, with accessory monazite and zircon (Figure 4). Quartz occurs as

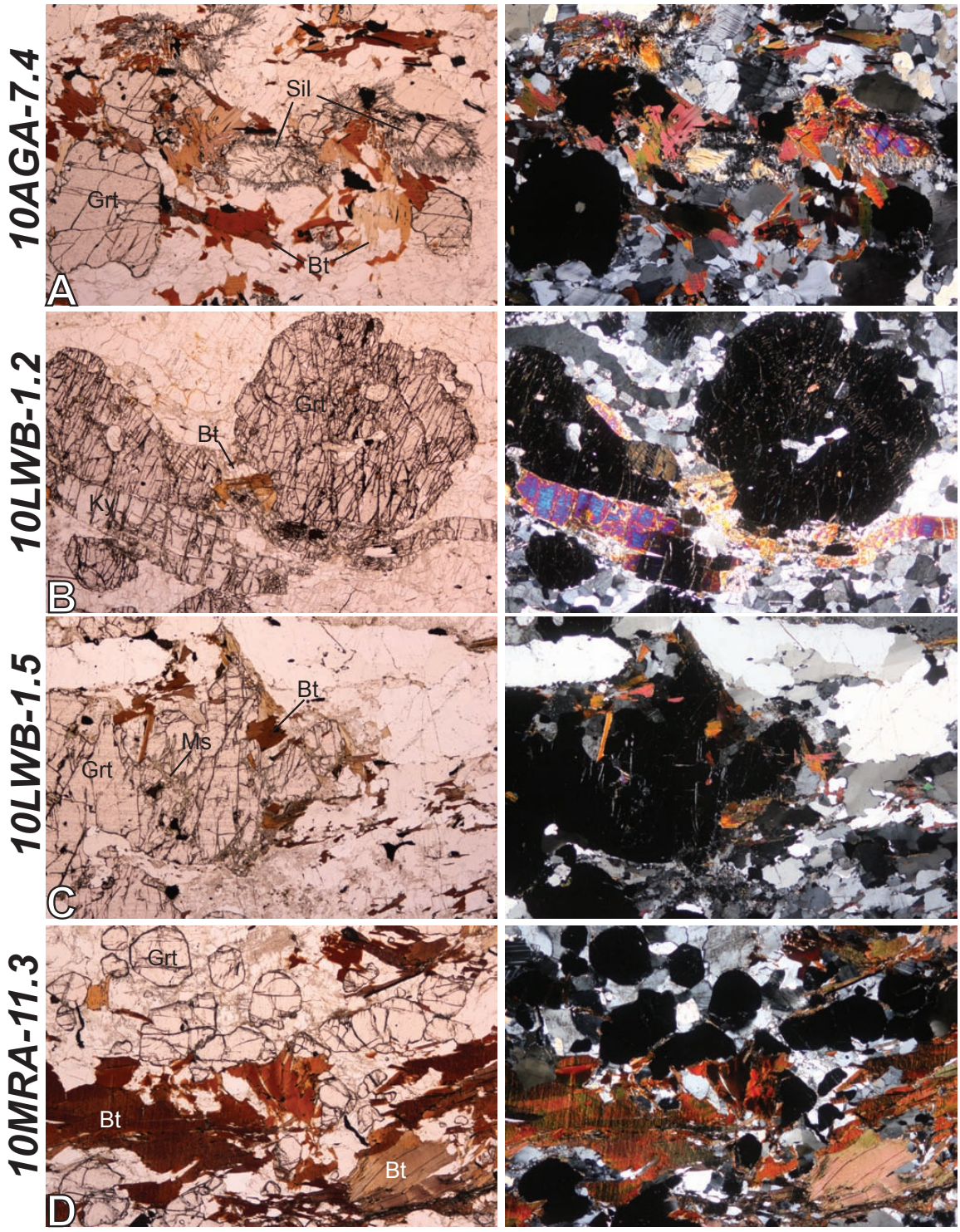

Figure 4: Large-scale thin section photomicrographs (FOV~11mm) with major metamorphic minerals labeled. . A) 10AGA-7.4; B) 10LWB-1.2; C) 10LWB-1.5; D) 10MRA-11.3. Grt= garnet, Bt= biotite, Sil= sillimanite, Ky= kyanite, Ms= muscovite. Left column is plane-polarized light and right column is cross-polarized light

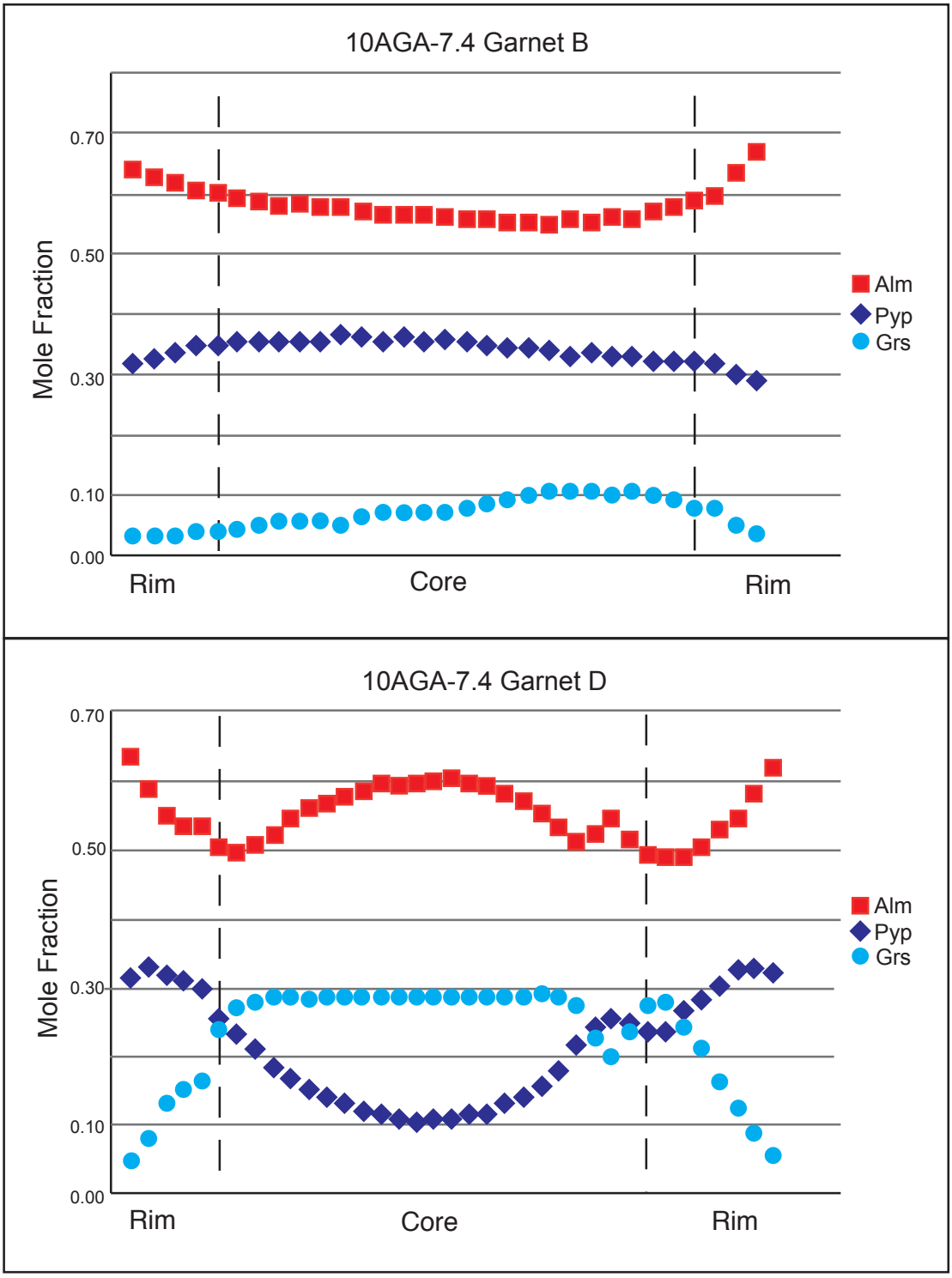

Figure 5: Electron microprobe garnet spot profiles for sample 10AGA-7.4. Alm= Almandine; Grs = Grossular; Pyp= pyrope; Spessartine content is negligible relative to other endmember components and was excluded from the graph. Vertical lines separate the prograde garnet growth domains from retrograde resorption. Peak P-T estimates were made from an average of points near the vertical line.

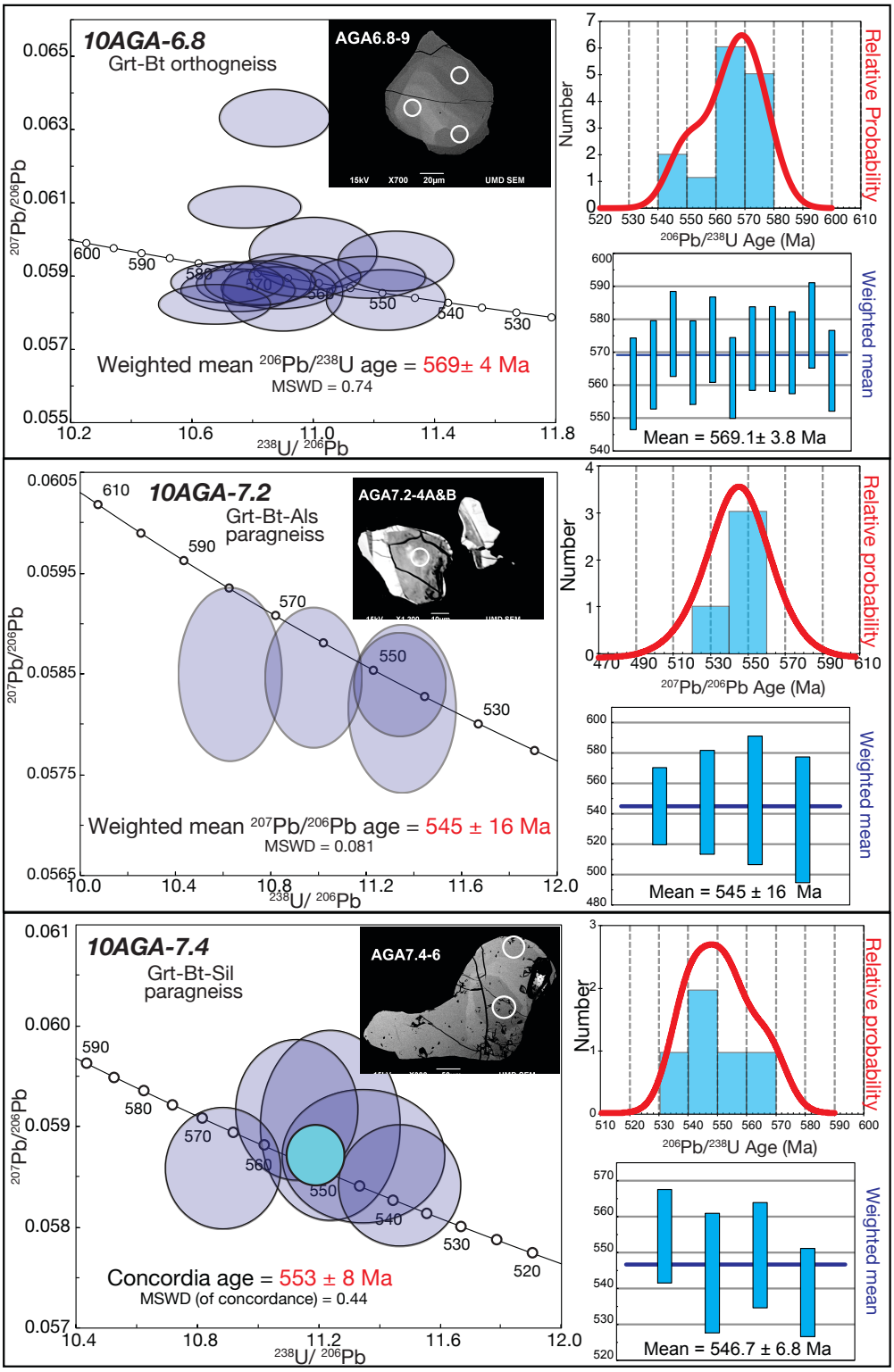

Figure 6: U-Pb age plots from dated metamorphic glacial clasts, with relative probability age distributions, weighted mean $^{207}Pb/^{206}Pb$ ages, and representative monazite BSE images. Circles on monazites show spot locations from SHRIMP-II. Box height on weighted-mean plots are 2σ.

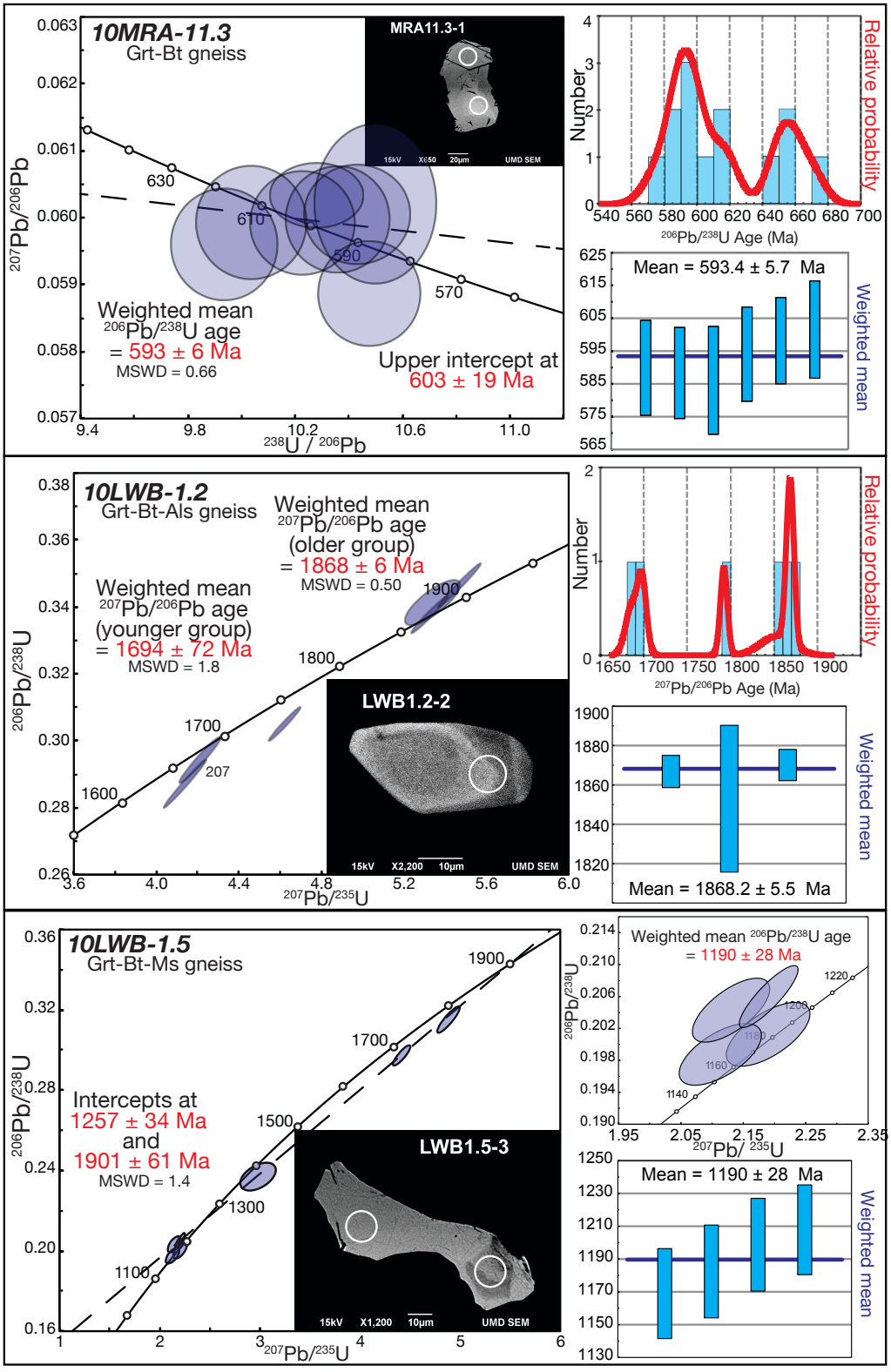

Figure 6: continued

inclusions in garnet and as ribbons in the matrix with undulose extinction. The average composition of plagioclase is An_{35} and the average composition of alkali feldspar is Or_{94}. Plagioclase is optically homogeneous and shows little compositional variation throughout the sample; the majority of grains show alteration.

Garnets, which range in size from 1-7 millimeters, are hypidioblastic and fractured, with inclusions of quartz, plagioclase, biotite, monazite and zircon. Garnets are oriented along the foliation and compositionally homogeneous with an average composition of $Alm_{58}Pyp_{35}Grs_5Sps_2$ (Appendix 1).

Biotite ranges from light to medium-dark brown color and occurs along foliation and edges of garnet, and as rare inclusions in garnet. Matrix biotite is dark brown with an average Mg/(Mg+Fe) ratio of 0.78. Biotite inclusions are light brown with an average Mg/(Mg+Fe) ratio of 0.67.

Kyanite forms coarse blades (0.5 -3.0 millimeters long) that are elongate along foliation and wrap around garnet. Kyanite shows fractures and lacks inclusions. Monazite grains (10-30 microns) occur as inclusions in garnet; backscattered electron images show patchy zoning (Fig. 6).

Table 1: Summary of *In-Situ* U-Pb Monazite Ages

Sample	# of Analyses	Type of Age	System	Age (Ma)	±	MSWD
10AGA-6.8	11	weighted mean	$^{206}Pb/^{238}U$	569	5	0.74
10AGA-7.2	4	weighted mean	$^{207}Pb/^{206}Pb$	545	16	0.08
10AGA-7.4	5	concordia	---	553	8	0.44
	4	weighted mean	$^{206}Pb/^{238}U$	547	7	1.09
10MRA-11.3	3	weighted mean	$^{206}Pb/^{238}U$	593	6	0.66
	8	T-W upper intercept	---	603	19	1.04
	3	older group	$^{206}Pb/^{238}U$	660 (est.)	---	---
10LWB-1.2	2	weighted mean	$^{207}Pb/^{206}Pb$	1694	72	1.80
	3	weighted mean	$^{207}Pb/^{206}Pb$	1868	6	0.50
10LWB-1.5	4	weighted mean	$^{206}Pb/^{238}U$	1190	28	1.60
	7	Wetherill regression	lower Intercept	1257	34	1.40
		Wetherill regression	upper Intercept	1901	61	1.40

Clast 10LWB-1.5

Clast 10LWB-1.5 is a fine-grained well-foliated garnet-biotite-muscovite gneiss (Figure 3). This clast is composed of quartz, plagioclase, alkali feldspar, garnet, biotite, and muscovite, with accessory rutile, monazite, and zircon (Figure 4). Quartz occurs as ribbons that, together with feldspar, define the foliation. Plagioclase is optically and chemically homogenous with an average composition of An_{30}. The average composition of alkali feldspar is Or_{91}.

Garnets, ranging in size from 2-10 millimeters, are hypidioblastic and contain quartz, plagioclase, muscovite, and monazite as inclusions. Garnet is compositionally homogenous with an average composition of $Alm_{59}Pyp_{34}Grs_{6}Sps_{1}$ (Appendix 1).

Biotite is pale brown with a slight green tint and an average Mg/(Mg+Fe) ratio of 0.67. Matrix biotite occurs along foliation and in small clusters that crosscut feldspars and quartz. Muscovite occurs as inclusions in garnet and does not appear in the matrix. Monazite (10-50 microns) occurs as inclusions in garnet; backscattered electron images show patchy zoning (Fig. 6).

Clast 10MRA-11.3

Clast 10MRA-11.3, a poorly-foliated garnet-biotite gneiss, is coarse-grained with 0.5-2.0 centimeter bands of lightly-colored feldspars alternating with bands of quartz, garnets and oxides (Figure 3). This clast is composed of quartz, plagioclase, garnet, and biotite, with accessory rutile, monazite and zircon

(Figure 4B). The quartz is fine- to medium-grained (0.1-0.5 millimeters) and occurs in the matrix and as inclusions in garnet. Plagioclase (An_{30}) is optically and chemically homogeneous.

Garnets, ranging size from 0.5 to 2.0 millimeters, are hypidioblastic with inclusions of quartz, plagioclase, and biotite. Garnets are chemically homogeneous with an average composition of $Alm_{65}Pyp_{29}Grs_{5}Sps_{1}$.

Biotite is a deep red with an average Mg/(Mg+Fe) ratio of 0.60. Biotite occurs along foliation and as radial growths crosscutting previous deformation fabric. Monazite grains are 40-100 μm and occur as inclusions within garnet; backscattered electron images show patchy zoning (Fig. 6).

Monazite U-Pb Geochronology

The closure temperature for naturally-occurring monazite is poorly constrained but is generally considered to be similar to zircon, between 900 and 1150 °C (Cherniak et al., 2004; Sajeev et al., 2010). For this study the high closure temperatures mean that monazite U-Pb ages probably correspond to the time of peak granulite-facies metamorphic crystallization.

We obtained U-Pb monazite ages for all seven metamorphic rock clasts. Because the ages were determined *in-situ* by ion microprobe on small grains, the number of grains available for analysis was limited. For six of the clasts, we analyzed 5-12 spots on multiple grains with a spot size of 10 microns. When possible, we analyzed different domains within monazites based on backscatter images. Monazites yielded uniform ages regardless of compositional domain

analyzed. SHRIMP U-Pb monazite ages for these clasts range from about 545 to 1900 Ma; most also show evidence of Ross Orogen-age metamorphism (~550 Ma). Results are summarized in Table 1 and shown in Figure 6. Individual sample results are listed in Appendix 2. Spot analyses from the seventh clast, 10AGA-6.1, yielded only Ross Orogen ages, so the results are not included for discussion below.

Four clasts collected from Argo Glaicer and Milan Ridge gave near concordant to concordant metamorphic ages consistent with the timing of Ross Orogen (Table 4). Sample 10AGA-7.2 has a weighted-mean $^{207}Pb/^{206}Pb$ age of 545 ± 16 Ma and sample 10AGA-7.4 has a concordia age of 553 ± 8 Ma and a weighted-mean $^{206}Pb/^{238}U$ age of 547 ± 7. Samples 10AGA-6.8 and 10MRA-11.3 have weighted-mean $^{206}Pb/^{238}U$ ages of 569 ± 4 and 593 ± 6 Ma, respectively;

Table 2: Electron microprobe analyses of representative garnet

Sample:	**10AGA-7.4**	**10AGA-7.4**	**10AGA-7.4**	**10AGA-7.4**	**10MRA-11.3**	**10MRA-11.3**	**10LWB-1.2**	**10LWB1.2**	**10LWB-1.5**
Location:	**Grt B Core**	**Grt B Edge**	**Grt D Core**	**Grt D edge**	**Grt A**	**Grt E**	**Grt A Core**	**Grt A Rim**	**Grt B Core**
Weight % Oxides									
SiO_2	39.51	39.05	38.65	38.81	38.64	38.75	39.24	39.05	39.39
TiO_2	0.08	0.68	0.09	0.10	0.02	0.03	0.02	0.00	0.03
Cr_2O_3	0.04	0.05	0.00	0.01	0.04	0.04	0.03	0.07	0.07
Al_2O_3	21.75	21.50	20.79	21.16	21.31	21.34	21.48	21.59	21.29
CaO	2.88	1.41	10.26	9.66	1.66	2.12	1.96	1.82	2.08
MgO	9.46	9.04	2.78	6.15	6.94	7.40	9.61	9.43	9.48
FeO	26.76	28.60	27.53	23.76	31.14	29.97	26.95	27.08	27.40
MnO	0.30	0.34	0.39	0.32	0.55	0.55	1.15	1.20	0.59
Total	100.79	100.68	100.47	99.96	100.30	100.20	100.43	100.40	100.32
Cations based on 12 O									
Si	3.01	3.00	3.04	3.01	3.02	3.02	3.01	3.01	3.02
Ti	0.00	0.04	0.01	0.01	0.00	0.00	0.00	0.00	0.00
Cr	0.00	0.00	0.00	0.00	0.00	0.00	0.00	0.00	0.00
Al	1.95	1.94	1.93	1.93	1.96	1.96	1.94	1.95	1.93
Ca	0.24	0.12	0.86	0.80	0.14	0.18	0.16	0.15	0.17
Mg	1.07	1.03	0.33	0.71	0.81	0.86	1.10	1.08	1.08
Fe	1.71	1.84	1.81	1.54	2.03	1.95	1.73	1.74	1.76
Mn	0.02	0.02	0.03	0.02	0.04	0.04	0.08	0.08	0.04
Total	8.01	7.99	7.99	8.02	8.00	8.00	8.02	8.01	8.01
End-Member Components									
Almandine	0.56	0.61	0.60	0.50	0.67	0.65	0.56	0.57	0.58
Pyrope	0.35	0.34	0.11	0.23	0.27	0.28	0.36	0.35	0.36
Spess	0.01	0.01	0.01	0.01	0.01	0.01	0.02	0.03	0.01
Gross	0.08	0.04	0.29	0.26	0.05	0.06	0.05	0.05	0.06
Mg#	0.39	0.36	0.15	0.32	0.28	0.31	0.39	0.38	0.38

Table 3: Electron microprobe analyses of representative micas

Sample:	10AGA-7.4	10AGA-7.4	10MRA-11.3	10MRA-11.3	10LWB-1.2	10LWB-1.2	10LWB-1.5	10LWB-1.5
Location:	Grt B Matrix	Grt D Matrix	Grt A Matrix	Grt E Matrix	Grt A core Inclusion	Grt A rim Matrix	Grt B Inclusion	Grt B Inclusion
Mineral:	Biotite	Biotite	Biotite	Biotite	Biotite	Biotite	Biotite	Muscovite
Weight % Oxides								
SiO_2	36.16	36.34	35.55	35.21	36.70	36.38	35.90	45.92
TiO_2	3.89	4.50	4.77	4.89	3.79	3.07	5.08	0.18
Al_2O_3	17.74	17.48	18.36	18.43	18.17	19.14	15.99	36.38
FeO	11.98	13.25	15.01	14.90	9.32	14.44	11.97	1.14
MnO	0.01	0.01	0.01	0.02	0.01	0.06	0.01	0.01
MgO	14.58	13.84	12.45	11.95	16.45	12.18	15.18	0.31
CaO	0.22	0.01	0.01	0.02	0.01	0.02	0.03	0.01
Na_2O	0.08	0.07	0.07	0.09	0.05	0.06	0.10	0.28
K_2O	9.97	10.16	10.04	9.93	11.30	10.82	11.22	11.24
Total	94.64	95.68	96.28	95.43	95.82	96.27	95.54	95.46
Cations Based on 22 O								
Si	5.376	5.621	5.29	5.23	5.46	5.41	5.34	6.83
Ti	0.434	0.455	0.53	0.55	0.42	0.34	0.57	0.02
Al	3.102	3.250	3.21	3.22	3.18	3.35	2.80	6.36
Fe	1.484	1.557	1.86	1.85	1.15	1.79	1.48	0.14
Mn	0.001	0.002	0.00	0.00	0.00	0.01	0.00	0.00
Mg	3.251	3.377	2.78	2.66	3.67	2.72	3.38	0.07
Ca	0.033	0.038	0.00	0.00	0.00	0.00	0.00	0.00
Na	0.024	0.025	0.02	0.03	0.02	0.02	0.03	0.08
K	1.891	1.976	1.91	1.88	2.15	2.05	2.13	2.13
Total	15.60	16.30	15.59	15.43	16.04	15.69	15.73	15.64
Mg/(Mg+Fe)	0.69	0.68	0.60	0.59	0.76	0.60	0.70	0.32

Table 4: Electron microprobe analyses of representative feldspars

Sample:	10AGA-7.4	10AGA-7.4	10AGA-7.4	10MRA-11.3	10MRA-11.3	10LWB-1.2	10LWB-1.2	10LWB-1.2	10LWB-1.5	10LWB-1.5
Location:	Grt B Matrix	Grt D Matrix	Grt D Matrix	Grt A Matrix	Grt E Matrix	Grt A Matrix	Grt A core Inclusion	Grt A rim Matrix	Grt B Matrix	Grt B Inclusion
Mineral:	Plag	Plag	K-Spar	Plag	Plag	K-Spar	Plag	Plag	K-Spar	Plag
Weight % Oxides										
SiO_2	58.39	58.39	63.92	60.61	60.20	63.29	58.19	59.49	64.71	60.99
Al_2O_3	25.44	25.26	17.96	24.61	24.32	18.54	25.11	25.29	18.43	24.44
FeO	0.10	0.01	0.03	0.10	0.06	0.12	0.13	0.17	0.27	0.10
MgO	0.00	0.00	0.01	0.00	0.00	0.00	0.01	0.00	0.00	0.00
CaO	8.02	8.02	0.09	6.28	6.14	0.09	7.64	7.31	0.08	6.42
Na_2O	6.85	6.84	0.58	7.89	7.86	0.79	7.09	7.51	1.15	7.97
K_2O	0.24	0.29	16.33	0.26	0.28	17.30	0.68	0.35	16.70	0.24
Total	99.03	98.82	98.91	99.75	98.85	100.14	98.84	100.11	101.34	100.16
Cations based on 8 O										
Si	2.64	2.64	3.00	2.70	2.71	2.95	2.64	2.66	2.97	2.71
Al	1.35	1.35	0.99	1.29	1.29	1.02	1.34	1.33	1.00	1.28
Fe	0.00	0.00	0.00	0.00	0.00	0.00	0.00	0.01	0.01	0.00
Mg	0.00	0.00	0.00	0.00	0.00	0.00	0.00	0.00	0.00	0.00
Ca	0.39	0.39	0.00	0.30	0.30	0.00	0.37	0.35	0.00	0.31
Na	0.60	0.60	0.05	0.68	0.69	0.07	0.62	0.65	0.10	0.69
K	0.01	0.02	0.98	0.01	0.02	1.03	0.04	0.02	0.98	0.01
Total	4.99	4.99	5.02	5.00	5.00	5.09	5.02	5.01	5.07	5.00
End-member components										
X_{An}	0.39	0.39	0.00	0.30	0.30	0.00	0.36	0.34	0.00	0.30
X_{Ab}	0.60	0.60	0.05	0.68	0.69	0.06	0.60	0.64	0.09	0.68
X_{Or}	0.02	0.03	0.95	0.02	0.02	0.94	0.06	0.03	0.91	0.02

Table 5: Results of P-T estimates from THERMOCALC

Sample Name	Minerals	Temperature (°C)	Pressure (kbar)	Correlation Coefficient*
10AGA-7.4 Grt B Core	Grt + Bt + Pl + Als	908 ± 88	12.3 ± 2	1.000
10AGA-7.4 Grt B Rim	Grt + Bt + Pl + Als	871 ± 132	11.4 ± 3	0.994
10AGA-7.4 Grt D Core	Grt + Bt + Pl + Als + Ksp	718 ± 120	13.2 ± 3	0.815
10AGA-7.4 Grt D Rim	Grt + Bt + Pl + Als + Ksp	825 ± 90	15.3 ± 2	0.780
10LWB-1.2 Grt A Core	Grt + Bt + Pl + Als + Ksp	865 ± 94	11.3 ± 2	0.992
10LWB-1.2 Grt A Rim	Grt + Bt + Pl + Als + Ksp	896 ± 90	12.0 ± 2	0.994
10LWB-1.5	Grt + Ms + Pl + Ksp	880 ± 182	12 ± 7	0.734

* Correlation coefficient from THERMOCALC for average P-T analysis

10MRA-11.3 also has an older subpopulation of ~660 Ma. Collectively these clasts record generally Ross-age metamorphism (550-600 Ma). However, these ages are significantly older than previous age constraints on Ross metamorphic activity based on $^{40}Ar/^{39}Ar$ and U-Pb ages for hornblende, muscovite, zircon and monazite (Goodge and Dallmeyer, 1992, 1996; Goodge et al., 1993; Goodge and Fanning, 1999), indicating that initiation of Ross orogenesis is likely earlier than previously thought.

Lonewolf Nunataks clasts 10LWB-1.2 and 10LWB-1.5 have monazite ages of 1190-1900 Ma with no evidence of Ross Orogen overprint. One grain analysis from sample 10LWB-1.5 was discarded for being negatively discordant, and the remaining analyses show minor lead loss and a weighted-mean $^{206}Pb/^{238}U$ age of 1190 ± 28 Ma. A Wetherill regression yields a lower intercept age of 1257 ± 34 Ma and upper intercept at 1901 ± 61 Ma. Sample 10LWB-1.2 has three reversely-discordant analyses that are not included in the age calculation. The remaining analyses show two populations with near-concordant $^{207}Pb/^{206}Pb$ ages of 1694 ± 72 Ma and 1868 ± 6 Ma. The Lonewolf Nunataks clasts show a metamorphic event at ~1900 Ma with overprints at ~1700 Ma and ~1200 Ma, corresponding in age to Nimrod and Grenville orogenic activity, respectively. To

our knowledge the older clast ages (~1900 Ma and ~1870 Ma) provide the first direct evidence of Paleoproterozoic metamorphism from central East Antarctica.

Thermobarometry

The compositions of co-existing garnet, biotite, plagioclase and muscovite in samples containing Al-silicate and quartz were used as input in the thermodynamic modeling program THERMOCALC to produce pressure and temperature estimates of metamorphism. Errors are estimated at the ~95% confidence level using double the standard deviation (as recommended by THERMOCALC tutorials). Two sets of mineral compositions were used to decipher the prograde metamorphic signatures during garnet growth: one to calculate conditions during early prograde growth (using garnet core compositions) and the other for peak P and T based on garnet rims. The prograde conditions were determined using an average of analyzed points from the center of each garnet coupled with inclusions of plagioclase and biotite within the same garnet. Garnet growth conditions were determined using rim garnet compositions and compositions of biotite and feldspar in contact with or near the edges of the garnet.

P-T estimates were derived through the optimization of end-member mineral reactions within a given pressure and temperature range using the average P-T analysis function. The simplest P-T calculations use single end-member reactions for equilibrium conditions (i.e Grt-Bt thermometer), whereas the average P-T calculation in THERMOCALC utilizes multiple independent

mineral equilibrium reactions within a given system using its internally consistent database. The system then becomes overdetermined (meaning there are more reactions than unknowns) and an average P-T estimate is derived using the least-squares method (see Holland and Powell, 1994 for further discussion). These calculations include calculated mineral activities and associated uncertainties and correlations. Multiple independent reactions, and their uncertainties, give a more robust P-T estimate versus single equilibrium reactions. Varying water content did not affect any of the calculations; thus water activity was assumed to be equal to 1.

Major element maps for the larger, less fractured garnets revealed no evidence of compositional variation in the Lonewolf Nunataks clasts (Appendix 1); however, garnet D in sample 10AGA-7.4 shows prograde metamorphic patterns, as discussed below (Appendix 1; Fig. 5). Representative mineral compositions used in P-T analysis are listed in Tables 2-4; P-T results for all of the samples are listed in Table 5 and shown in Figure 7.

Argo Glacier

Clast 10AGA-7.4 records high-pressure granulite-facies metamorphism indicative of crustal thickening or an orogenic event akin to Ross Orogen activity as indicated by monazite U-Pb age. In this sample, Garnet B shows minor elemental zoning, and the general trends of higher X_{Fe} toward the rims may be interpreted as a retrograde elemental signature (Fig. 5; Tuccillo et al., 2014). Garnet B core compositions yield a pressure of 12.3 ± 2 kbar and temperature of

908 ± 88 °C, whereas the edge composition yielded a pressure of 11.4 ± 3 kbar and temperature of 871 ± 134 °C. Element maps of garnet D, coupled with a traverse across the garnet, yielded prograde metamorphic patterns with increasing Mg and decreasing Ca, Fe, and Mn from the core (Appendix 1; Figs. 5). Garnet D core analyses yielded a pressure of 13.2 ± 3 kbar and temperature of 718 ± 120 °C and the edge composition yielded a pressure of 15.3 ± 2 and

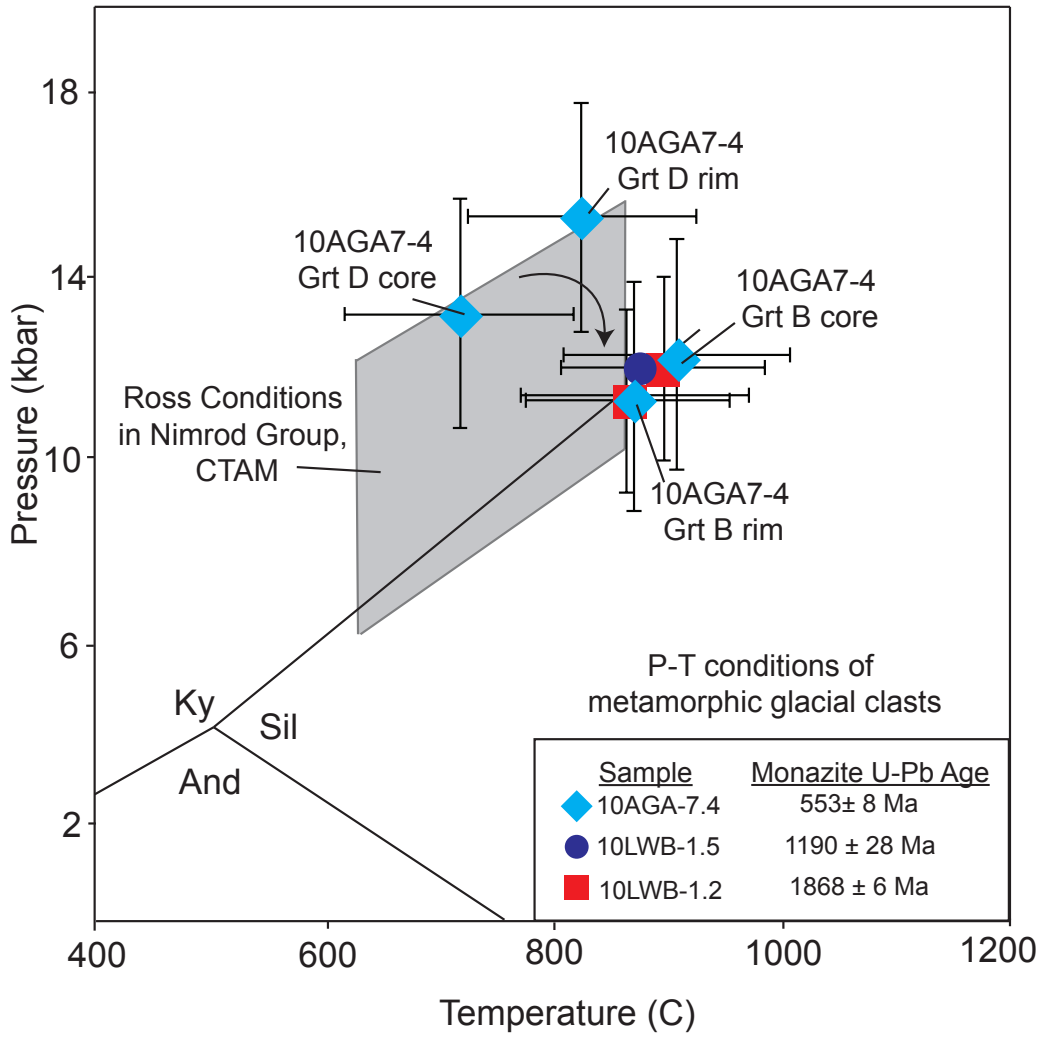

Figure 7: Pressure-temperature results with Al-silicate reaction boundaries (Ky= Kyanite; Sil= Sillimanite; And= Andalusite; Holdaway, 1971). Grey box indicates previously documented P-T results for Ross Orogen basement rocks (Nimrod Group; Goodge, 2007).

temperature of 825 ± 90 °C, indicating a possible prograde change to higher P and T. Garnet D has anomalously high calcium content relative to garnet B (Table 2).

Both garnets from 10AGA-7.4 exhibit evidence of resorption at the edges; therefore rim conditions were estimated from compositions taken at the compositional inflection (marked by vertical lines, Fig. 5) to ensure meaningful results. Pressure conditions estimated from garnets in this sample fall within error of each other. However, the minor zoning in garnet B suggests a partial late-stage thermal re-equilibration. As temperature increases and pressure decreases, garnet will preferentially lose calcium, as seen in this sample relative to both garnets analyzed from core to rim. Garnet B exhibits lower pressures than garnet D, consistent with retrograde conditions, as well as higher temperatures at the rims indicating post peak-pressure heating, common in clock-wise P-T paths associated with orogenic events. Garnet B may preserve later-stage continuous garnet growth versus garnet D, which preserves prograde to peak conditions (Tuccillo et al 1990).

Lonewolf Nunataks

Proterozoic age signatures were determined for two Lonewolf Nunataks clasts. Element maps from both clasts showed homogeneous compositions (Appendix 1). In sample 10LWB-1.2, garnet A core compositions yielded a pressure of 11.3 ± 2 kbar and a temperature of 865 ± 94 °C; rim compositions gave a pressure of 12.0 ± 2 kbar and temperature of 896 ± 90 °C. Core

compositions of garnet C yielded a pressure of 13.3 ± 0.4 kbar and a temperature of 914 ± 232 °C. Due to the anomalous errors for garnet C, further discussion disregards these results. Monazite U-Pb ages of 1700-1870 Ma for sample 10LWB-1.2 indicate that these high-pressure, granulite-facies metamorphic conditions document a Paleoproterozoic orogenic event somewhere within the EAS.

In sample 10LWB-1.5, garnet B yielded a pressure of 13.4 ± 5 kbar and a temperature of 889 ± 76 °C. There are no P-T calculations using the rim compositions of garnet B due to a lack of Al-silicates and muscovite in the matrix. This sample preserves high-pressure granulite-facies metamorphism and yields Paleoproterozoic age signatures with a Mesoproterozoic overprint. Garnets from sample 10LWB-1.5 show no elemental zoning signifying re-equilibration at high temperatures. Therefore, metamorphic conditions preserved in this sample are likely associated with the younger Mesoproterozic orogenic activity.

Milan Ridge

Clast 10MRA-11.3 contains no minerals useful as barometers (e.g. Al-silicates or muscovite), thus only temperature estimates could be determined, and pressure must be assumed. Because the age of the clast corresponds to the onset of the Ross Orogeny, pressures were assumed to be similar to previous estimates derived from Ross basement rock in the Nimrod Group (7-14 kbar; Goodge, 2007). For simplicity, this sample was analyzed using Spear's

GeoThermoBarometry (GTB) program with the Ferry & Spear (1978) garnet-biotite thermometer calibration.

To evaluate this sample, three different pressures were assumed: minimum Ross conditions at 7 kbar, maximum Ross conditions at 14 kbar, and an intermediate pressure of 10.5 kbar. The core of garnet A yielded temperatures between 695 ˚C at 7 kbar and 760 °C at 14 kbar, and a temperature of 744 °C at 10.5 kbar. The edge of garnet A yielded temperatures of 840 ˚C at 7 kbar to 875 °C at 14 kbar, and ~858 °C at 10.5 kbar. Average core compositions at 10.5 kbar for garnet E resulted in a temperature of ~895 °C whereas edge analysis yielded ~904 °C. Garnet A has fewer metamorphic reaction textures between the garnet and biotite, which leads to a more confident analysis. Temperature estimates are interpreted as peak temperatures, due to evidence of high-temperature elemental diffusion and re-equilibration within the clast.

Discussion

In this we study analyzed seven metamorphic glacial rock clasts collected from moraines adjacent to the central TAM (Fig. 2). Clasts were likely eroded from central East Antarctica via the Byrd Glacier catchment area (Fig. 1) and provide new insights to understanding geologic events that affected the ice-covered bedrock. U-Pb monazite ages show two major metamorphic signatures: Ross-age orogenesis (~660-550 Ma), and Paleoproterozoic metamorphism (~1900-1700 Ma) with a Mesoproterozoic overprint (~1200 Ma). Mineral compositions and petrologic data yield high-pressure and temperature conditions

for both the Ross-age and Paleoproterozoic events. The significance of these results with respect to the crustal evolution of central EAS and its role in supercontinent evolution is discussed below.

Ross Orogen Metamorphism

New monazite age data indicate that Ross metamorphism may have been initiated earlier than previously thought (Goodge and Dallmeyer, 1992; Goodge et al., 1993; Goodge, 2007). Five clasts, from Argo Glacier and Milan Ridge, yield Neoproterozoic monazite U-Pb ages (~595-545 Ma). Three clasts (10AGA-6.1, 10AGA-7.2 and 10AGA-7.4) have metamorphic ages of ~555-545 Ma; two clasts (10AGA-6.8 and 10MRA-11.3) have ages between ~570 and ~595 Ma. The latter, 10MRA-11.3, has an older monazite age population at ~660 Ma.

Texturally and mineralogically these samples resemble typical Ross Orogen metamorphic lithologies. Nimrod Group metamorphic rocks affected by the Ross Orogeny exhibit syn-kinematic kyanite + garnet + biotite ± muscovite, which is also evident in the Ross-age samples in this study. Clast 10AGA-7.4 also shows late-stage sillimanite growth, typical of Ross Orogen metamorphism in pelitic rocks of the Nimrod Group (Goodge, 2007). Thermobarometric calculations for sample 10AGA-7.4 (~13 kbar and ~800 °C) are similar to early Ross (~540 Ma) estimates (~8-12 kbar and 750-850 °C; Fig. 7). These high P-T conditions are consistent with crustal thickening associated with plate convergence.

Igneous and metamorphic ages between ~595-590 Ma (Goodge et al., 2012b; this study) pre-date previous age estimates of Ross activity and furthermore link early igneous and metamorphic events. The oldest previously published ages attributed to Ross-age metamorphism in the Nimrod Group are ~525 Ma ($^{40}Ar/^{39}Ar$ cooling ages of hornblende; Goodge and Dallmeyer, 1992) and ~520 Ma (U-Pb dating of monazite; Goodge et al., 1993). Studies of detrital zircons and glacial clasts indicate that Ross Orogen-related magmatic activity was initiated as early as ~590 Ma (Goodge et al., 2004, 2012). Overall, a long sequence of events between about 595-480 Ma reflects a multi-phase protracted Ross Orogen cycle (Goodge et al., 1993; Goodge, 1997; 2007).

If the lithologic and petrologic characteristics of the glacial clasts correlate with basement rocks of the Ross Orogen, then their ages suggest a younging trend of metamorphism from west to east across the TAM toward the present Ross Sea. This trend parallels the progression of Ross granite emplacement with inboard magmatic activity starting at ~545 Ma and post-kinematic activity (515-480 Ma) moving outboard (east) over time (Goodge et al., 2012). Thus, old metamorphic ages in these clasts may represent a subglacial Ross Orogen metamorphism farther inland than previously thought (Fig. 8A).

Clast 10MRA-11.3 has monazite age populations of ~600 Ma and ~660 Ma. Likewise, Neoproterozoic volcanic rocks with ages of ~670 Ma in the central TAM and ~650 Ma in southern Victoria Land likely indicate rift-related magmatism associated with the break-up of Rodinia (Goodge et al., 2002; Cooper et al., 2011). The late Neoporterozoic age signature in Sample 10MRA-11.3 may reflect

high-temperature rift-type metamorphism in the lower crust associated with this tectonic phase in the transition from break-up to active-margin convergence (Goodge et al., 2004).

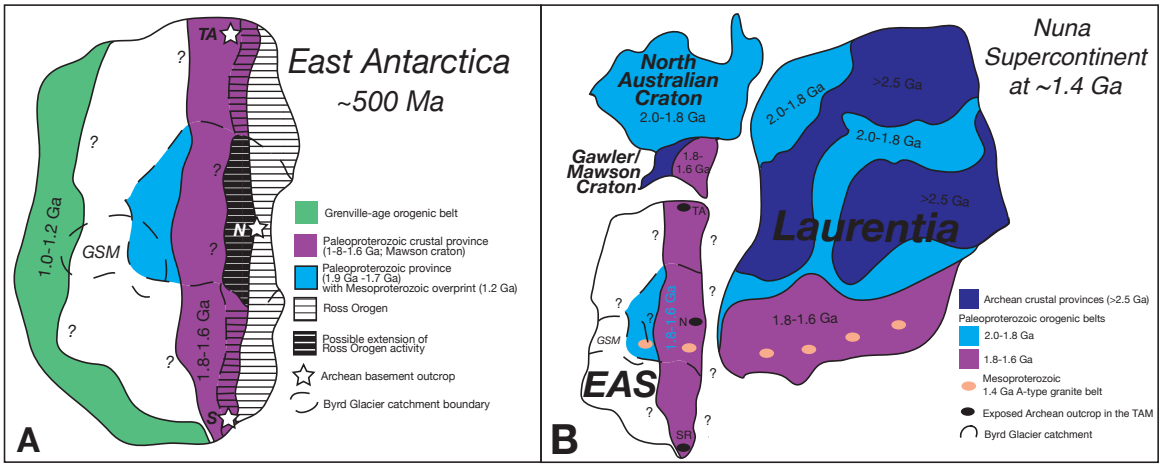

Figure 8: A) Generalized reconstruction of crustal provinces in East Antarctica. New findings from this study include: extension of Ross Orogen activity inboard of the present-day TAM, the presence of Mesoproterozoic metamorphic crust, and possible Proterozoic metamorphic crust beneath the ice within the Byrd Glacier catchment and under the GSM. Major Archean outcrops (stars) include Terre Adélie (TA), Nimrod Group (N), and the Shackleton Range (S). Boundaries of each province are approximate. B) Generalized paleogeographic reconstruction of East Antarctica with respect to Australia and Laurentia in the Nuna supercontinent, with speculated crustal provinces and boundaries, and extension of Paleoproterozoic crust beneath the Byrd Glacier catchment and GSM. Black ellipses indicate exposed Archean outcrop in Terre Adélie (TA), the Nimrod group (N) near the Miller Range, and the Shackleton Range (SR). Note that Ross, Grenvillian and Pan-African orogens have been removed. Modified after Boger (2011), Goodge (2001), and Fitzsimons (2003).

Paleoproterozoic metamorphism and Mesoproterozoic overprints

Metamorphic glacial clast samples from Lonewolf Nunataks (10LWB-1.2 and 10LWB-1.5) yield Proterozoic ages, which, when coupled with high-grade P-T estimates, indicate a previously unknown geologic province with unique tectonothermal characteristics located beneath the ice. Clast 10LWB1.2 yielded ages of ~1870 and ~1700 and clast 10LWB-1.5 yielded an age of 1190 Ma with an age component at ~1900 Ma. The ages of these metamorphic clasts are

similar to ages obtained from some igneous glacial clasts, also collected from the Byrd Glacier catchment. The igneous ages range from Paleoproterozoic (~1580 Ma, ~1880 Ma, and ~2000 Ma) to Mesoproterozoic (~1000- ~1250 Ma and ~1440-1460 Ma; Goodge et al., 2010; Goodge et al., 2012b). Together, a coherent age suite of Proterozoic igneous and metamorphic glacial clasts indicates a previously unknown Paleoproterozoic crustal province within the EAS.

The Lonewolf Nunataks samples presented in this study were metamorphosed under eclogite/high-pressure granulite-facies metamorphic conditions (~860-900°C and ~11-12 kbar; Fig. 7). Eclogite/high-pressure granulite-facies rocks typically lack orthopyroxene and experience late-stage heating that erases any record of a prograde path (O'Brien and Rötzler, 2003), as occurs in the Lonewolf Nunataks samples. This Paleoproterozoic eclogite/high-pressure granulite-facies metamorphism, characterized by a geothermal gradient of ~20°C/km, resembles a pre-modern thickening tectonic regime that coincides with the formation of early supercontinents, including Nuna and Rodinia (Brown, 2006).

Central East Antarctica lacks direct evidence to determine its role in the early amalgamation and existence of the Nuna supercontinent (~1.9-1.4 Ga), Paleoproterozoic ages and high P-T estimates from glacier clasts may reflect tectonic activity associated with crustal thickening and formation of the Nuna supercontinent within the Antarctic portion of the Mawson craton. Similar age Paleoproterozoic crustal provinces are reported from Laurentia (Condie, 1982; Bennett and DePaolo, 1987; Strickland et al., 2013), with major crustal accretion

events from 1800-1600 Ma (Condie, 1982). A-type Rapakivi granites of ~1400 Ma from studies in both Laurentia and East Antarctica indicate a possible paleogeographic connection (Goodge et al., 2008); however, it is unclear if these granites are the product of rifting or amalgamation (Anderson and Morrison, 2005; Goodge and Vervoort, 2006; Goodge et al., 2010). Age similarities of ancient crustal provinces may show a possible connection of the Mawson craton (EAS-Australia) and Laurentia during the evolution of Nuna supercontinent between ~1.9 – 1.4 Ga (Fig. 8B).

Igneous and metamorphic glacial clasts collected from the Byrd Glacier catchment also indicate a distinctive Mesoproterozoic (Grenville-age) overprinting event of ~1250-1000 Ma that extends inboard of the TAM underneath the ice (Goodge et al., 2010; this study). Previous studies support Grenville-age (1300-900 Ma) orogenic belts extending into the interior of the EAS, based on coastal outcrops and their affinities with India, Africa and Australia (Fig. 1; Fitzsimons, 2000; Boger, 2011). Collision between the western Australia craton/ South Australian craton with the western edge of the Mawson craton (during the Albany-Fraser Orogeny) is documented to have occurred in two stages; the first between 1340 Ma and 1260 Ma, and the second between 1215 Ma and 1140 Ma (Clark et al., 2000; Fitzsimons, 2000; Boger, 2011). Sample 10LWB-1.5 has a monazite age of ~1190 Ma, with an older ~1250 Ma component. This Mesoproterozoic age signature, coupled with high P-T metamorphic conditions indicative of orogenic activity, documents an overprint that may be associated with the early amalgamation of Rodinia, possibly by

extension of the Albany-Fraser Orogeny into the interior of the EAS beneath the East Antarctic ice sheet.

Gamburtsev Subglacial Mountains

The formation of the Gamburtsev Subglacial Mountains remains enigmatic. High-density crustal roots imaged seismically beneath this mountain massif and lack of recent (<480 Ma) volcanic activity implies an orogenic collisional belt beneath the ice in the EAS, rather than an active mantle source (Van der Flierdt et al., 2008; Ferracioli, 2011). No direct age data from the Gamburtsev Subglacial Mountains exist, but it is estimated that the mountains were formed prior to Pan-African orogenic events associated with the formation of Gondwana. Because part of these mountains lay within the Byrd Glacier catchment area (Fig.8A), the Lonewolf Nunataks clasts may help constrain the timing and nature of crustal events associated with them. However, further study is needed to understand the role of the Gamburtsev Subglacial Mountains, if any, during supercontinent formation, as well as extension of Paleoproterozoic to Neoproterozoic crust to the interior of the EAS.

Conclusions

Glacial metamorphic rocks clasts eroded from the East Antarctic interior may serve as proxy samples for the ice-covered craton. Five clasts of high-grade gneisses, from moraines near the Miller Range, yielded Neoproterozoic monazite U-Pb ages ranging from ~595-545 Ma, and one has an older age population of

~660 Ma. These Ross Orogen-age clasts experienced high-temperatures (700-900 °C) and pressures (~11-15 kbar) consistent with previously estimated Ross-age metamorphic conditions for the Nimrod Group (Goodge, 2007). Assuming a linear relationship between temperature and depth in the crust, these clasts reflect a metamorphic geotherm of ~19°C/km, which is consistent with crustal thickening associated with Ross Orogen convergence. The similarity in rock types, mineral assemblages, P-T conditions, metamorphic geotherm and ages indicates that glacially eroded crystalline basement of the EAS was affected by the Ross Orogeny some distance inboard of present exposure of the Nimrod Group (Fig. 8A). Orogenic effects on this basement are imaged as much as ~100 km inboard of the presently exposed TAM beneath the East Antarctic ice sheet (Goodge and Finn, 2010).

Metamorphic ages of 595-545 Ma in clasts with characteristic Ross petrography and metamorphic signatures inboard from the TAM also indicate an earlier onset of Ross Orogen metamorphism than recorded in basement exposure. Ross activity therefore appears to be diachronous, younging from inboard to outboard of the TAM toward the Ross Sea; this pattern is also recognized in the sequence of deformation observed in low-grade rocks of the Robertson Bay Group in northern Victoria Land (Dallmeyer and Wright, 1992; Goodge, 2007), as well as the timing of granite emplacement in the central TAM (Goodge et al., 2012).

Clasts from Lonewolf Nunataks have Paleoproterozoic ages and no evidence of Ross Orogen-age metamorphic overprint. Lonewolf Nunataks

samples have ages of 1900-1700 Ma with a Mesoproterozoic overprint at ~1200 Ma. These clast ages are anomalous with respect to outcrop ages obtained elsewhere in Antarctica and signify a previously unrecognized tectonothermal event in the subglacial geology of East Antarctica. Pressure-temperature conditions for these samples (~865-900 °C and ~11-12 kbar) correspond with a metamorphic geotherm of about 23°C/ km, which is indicative of orogenic activity associated with crustal thickening, assuming a linear crustal geotherm. Because eclogite high-pressure granulite-facies conditions were prevalent during supercontinent formation during the Proterozoic, notably during the amalgamation of Nuna and Rodinia (Brown, 2006), the Lonewolf Nunataks samples may therefore reflect crustal thickening due to Proterozoic craton convergence during supercontinent assembly.

Cratonic East Antarctica is thought to have a three-stage tectonic history (Fitzsimons, 2000): 1) craton stabilization (before 1700 Ma); 2) Meso- to Neoproterozoic (1130-1330 Ma) mobile-belt activity that has overprinted underlying Archean crust, effectively suturing the marginal cratons (India, Africa and Australia) with the EAS; and 3) Ross and Pan-African orogenic activity (600-500 Ma), which thermally and structurally overprinted much of Antarctica's exposed geologic history. Metamorphic glacial clasts from this study exhibit age signatures from each of these time periods, with high-grade events from ~1900-1700 Ma, metamorphic overprinting at ~1200 Ma, and Ross Orogen-age events from ~660-550 Ma. By extrapolation, newly recognized Proterozoic crustal

activity in East Antarctica may have led to the formation of the Gamburtsev Subglacial Mountains, which exhibits a cold, thick crustal root (Fig. 8A). Furthermore, these glacial clasts correspond in age with distinctive orogenic belts in other ancient cratons and may imply an early connection between East Antarctica, Laurentia and the Northern Australia and Gawler cratons as a coherent block during formation of the Nuna supercontinent (Fig. 8B). It is possible, for example, that the Paleoproterozoic metamorphic age signatures reported here may correspond to orogenic activity related to Nuna amalgamation recorded in the Trans-Hudson orogen of Laurentia.

Reconstructions of Nuna and Rodinia often neglect the EAS, due to a lack of knowledge about its subglacial geology; however, metamorphic glacial clasts, potentially carried from the interior of the EAS, for the first time record Paleoproterozoic (~1900-1700 Ma), Mesoproterozoic (~1260- 1190 Ma) and early Ross Orogen-age (660-545 Ma) metamorphic events that help inform us about the otherwise hidden crustal history. This metamorphic history complements previously documented igneous clast ages obtained from the Byrd Glacier catchment (Goodge et al., 2010; Goodge et al., 2012). Further documentation of P-T conditions and metamorphic ages from glacial clasts may help to reveal the enigmatic geology from large areas of the ice-covered EAS. Additionally, further study in the EAS will clarify the role of East Antarctica and the Gamburtsev Subglacial Mountains during evolution of the Nuna and Rodinia supercontinents.

Bibliography

Bennett, V.C., and Depaolo, D.J., 1987, Geological Society of America Bulletin Proterozoic crustal history of the western United States as determined by neodymium isotopic mapping, Geological Society of America Bulletin, v. 99, p. 674–685, doi: 10.1130/0016-7606(1987)99<674.

Bennett, V.C., and Fanning, C.M., 1993, A Glimpse of the cryptic Gondwana shield: Archean and Proterozoic ages from central Transantarctic Mountains: Geological Society of America Abstract with programs, v. 25, p. 49.

Boger, S.D., 2011, Antarctica - Before and after Gondwana: Gondwana Research, v. 19, p. 335–371, doi: 10.1016/j.gr.2010.09.003.

Boger, S.D., Wilson, C.J.L., and Fanning, C.M., 2001, Early Paleozoic tectonism within the East Antarctic craton: The final suture between east and west Gondwana?: Geology, v. 29, p. 463, doi: 10.1130/0091-7613(2001)029<0463.

Borg, S.G., and DePaolo, D.J., 1994, Laurentia, Australia, and Antarctica as a Late Proterozoic supercontinent: Constraints from isotopic mapping: Geology, v. 22, p. 307, doi: 10.1130/0091-7613(1994)022<0307.

Cawood, P. a., 2005, Terra Australis Orogen: Rodinia breakup and development of the Pacific and Iapetus margins of Gondwana during the Neoproterozoic and Paleozoic: Earth-Science Reviews, v. 69, p. 249–279, doi: 10.1016/j.earscirev.2004.09.001.

Condie, K.C., 1982, Geology Plate-tectonics model for Proterozoic continental accretion in the southwestern United States Plate-tectonics model for Proterozoic continental accretion in the southwestern United States: Geology, v. 10, p. 37–42, doi: 10.1130/0091-7613(1982)10<37.

Dallmeyer, R.D., and Wright, T.O., 1992, Diachronous cleavage development in the Robertson Bay Terrane, Northern Victoria Land, Antarctica: Tectonic implications: Tectonics, v. 11, no. 2, p. 437–448, doi: 10.1029/91TC02891.

Fanning, C.M., Daly, S.J., Bennett, V.C., Menot, R.P., Peucat, J.J., Oliver, R.L., and Monnier, O., 1995, The “Mawson Block”: once contiguous Archaean to Proterozoic crust in the East Antarctic shield and Gawler Craton: VII International Symposium on Antarctic Earth Sciences, Sienna, Italy,, p. 124.

Fanning, C.M.; Reid, A. J.; Teale, G.S., 2007, A geochronological framework for the Gawler Craton, South Australia: South Australia. Geological Survey, Bulletin 55, p. 1–258.

Ferraccioli, F., Armadillo, E., Jordan, T., Bozzo, E., and Corr, H., 2009, Aeromagnetic exploration over the East Antarctic Ice Sheet: A new view of the Wilkes Subglacial Basin: Tectonophysics, v. 478, p. 62–77.

Ferraccioli, F., Finn, C. a, Jordan, T. a, Bell, R.E., Anderson, L.M., and Damaske, D., 2011, East Antarctic rifting triggers uplift of the Gamburtsev Mountains: Nature, v. 479, p. 388–92, doi: 10.1038/nature10566.

Ferry, J.M., and Spear, F.S., 1978, Experimental calibration of the partitioning of Fe and Mg between biotite and garnet: Contributions to Mineralogy and Petrology, v. 66, p. 113–117.

Fitzsimons, I.C.W., 2003, Proterozoic basement provinces of southern and southwestern Australia, and their correlation with Antarctica: Geological Society, London, Special Publications, v. 206, p. 93–130.

Goodge, J.W., 2007, Metamorphism in the Ross orogen and its bearing on Gondwana margin tectonics: Geological Society of America Special Paper, 419, p. 185–203, doi: 10.1130/2006.2419(10).

Goodge, J.W., and Dallmeyer, R.D., 1992, 40Ar/39Ar Mineral Age Constraints on the Paleozoic Tectonothermal Evolution of High-Grade Basement Rocks within the Ross Orogen, Central Transantarctic Mountains: The Journal of Geology, v. 100, p. 91–106.

Goodge, J.W., and Fanning, C.M., 1999, 2.5 b.y. of punctuated Earth history as recorded in a single rock: Geology, v. 27, p. 1007–1010, doi: 10.1130/0091-7613(1999)027<1007.

Goodge, J.W., Fanning, C.M., and Bennett, V.C., 2001, U-Pb evidence of ~1.7 Ga crustal tectonism during the Nimrod Orogeny in the Transantarctic Mountains, Antarctica: Implications for Proterozoic plate reconstructions: Precambrian Research, v. 112, p. 261–288.

Goodge, J.W., Fanning, C.M., Brecke, D.M., Licht, K.J., and Palmer, E.F., 2010, Continuation of the Laurentian Grenville Province across the Ross Sea Margin of East Antarctica: The Journal of Geology, v. 118, p. 601–619, doi: 10.1086/656385.

Goodge, J.W., Fanning, C.M., Norman, M.D., and Bennett, V.C., 2012, Temporal, Isotopic and Spatial Relations of Early Paleozoic Gondwana-Margin Arc Magmatism, Central Transantarctic Mountains, Antarctica: Journal of Petrology, v. 53, p. 2027–2065, doi: 10.1093/petrology/egs043.

Goodge, J.W., Fanning, C.M., Vervoort, J.D., and Radakovich, A.L., 2012b, More SWEAT: Discovery of Mesoproterozoic and Paleoproterozoic igneous crust in East Antarctica strengthens the case for Laurentia-Antarctica connections in Rodinia: Geological Society of America Abstracts with Programs, v. 44, p. 599.

Goodge, J.W., and Finn, C. a., 2010, Glimpses of East Antarctica: Aeromagnetic and satellite magnetic view from the central transantarctic mountains of East Antarctica: Journal of Geophysical Research B: Solid Earth, v. 115, p. B09103, doi: 10.1029/2009JB006890.

Goodge, J.W., Hansen, V.L., and Peacock, S.M., 1992, Multiple petrotectonic events in high-grade metamorphic rocks of the Nimrod group, central Transantarctic Mountains, Antarctica, in Yoshida, Y., Kaminuma, K., and

Shiraishi, K., eds.,: Recent Progress in Antarctic Earth Science: Tokyo, Terra Scientific,, p. 203–209.

Goodge, J.W., Hansen, V.L., Peacock, M., Smith, B.K., and Walker, W., 1993, Kinematic evolution of the Miller Range shear zone, central Transantarctic Mountains, Antarctica, and implications for Neoproterozoic to early Paleozoic tectonics of the East Antarctic margin of Gondwana: Tectonics, v. 12, p. 1460–1478.

Goodge, J.W., Vervoort, J.D., Fanning, C.M., Brecke, D.M., Farmer, G.L., Williams, I.S., Myrow, P.M., and Depaolo, D.J., 2008, A positive test of East Antarctica-Laurentia juxtaposition within Rodinia supercontinent: Science, v. 321, p. 235–240.

Grindley, G.W., McGregor, V.R., and Walcott, R.I., 1964, Outline of the geology of the Nimrod-Beardmore-Axel Heiberg Glaciers region, Ross Dependency. In: Adie, R.J. (ed.): Antarctic Geology. North Holland Publishing Company, Amsterdam,,, p. 206.

Harley, S.L., and Kelly, N.M., 2007, Ancient Antarctica: the Archaean of the East Antarctic Shield: Developments in Precambrian Geology, v. 15, doi: 10.1016/S0166-2635(07)15032-5.

Hoffman, P.F., 1991, Did the Breakout of Laurentia Turn Gondwanaland Inside-Out ?: Science, v. 252, p. 1409–1412.

Holland, T.J.B., and Powell, R., 1985, An internally consistent thermodynamic dataset with uncertainties and correlations. II. Data and results.: Journal of Metamorphic Geology, v. 3, p. 343–370.

Jordan, T. a., Ferraccioli, F., Armadillo, E., and Bozzo, E., 2013, Crustal architecture of the Wilkes Subglacial Basin in East Antarctica, As revealed from airborne gravity data: Tectonophysics, v. 585, p. 196–206, doi: 10.1016/j.tecto.2012.06.041.

Lawrence, J.F., Wiens, D.A., Nyblade, A. A. Anandakrishan, S., Shore, P.J., and Voigt, D., 2006, Upper mantle thermal variations beneath the Transantarctic Mountains inferred from teleseismic Swave attenuation:: Geophysical Research Letters, v. 33.

Li, Z.X., Bogdanova, S.V., Collins, a. S., Davidson, a., De Waele, B., Ernst, R.E., Fitzsimons, I.C.W., Fuck, R. a., Gladkochub, D.P., Jacobs, J., Karlstrom, K.E., Lu, S., Natapov, L.M., Pease, V., et al., 2008, Assembly, configuration, and break-up history of Rodinia: A synthesis: Precambrian Research, v. 160, p. 179–210, doi: 10.1016/j.precamres.2007.04.021.

Moores, E.M., 1991, Southwest U . S . -East Antarctic (SWEAT) connection : A hypothesis: Geology, v. 19, p. 425, doi: 10.1130/0091-7613(1991)019<0425.

O’Brien, P.J., and Rotzler, J., 2003, High-pressure granulites : formation , recovery of peak conditions and implications for tectonics: Journal of Metamorphic Geology, v. 21, p. 3–20.

Oliver, R.L., and Fanning, C.M., 2002, Proterozoic geology east and southeast of Commonwealth Bay, George V Land, Antarctica, and its relationship to that of adjacent Gondwana terranes, in Gamble, J.A., Skinner, D.N.B., and Henrys, S., (eds.),: Antarctica at the Close of the Millennium: Wellington, New Zealand, Royal Society of New Zealand Bulletin, v. 35, p. 51–58.

Payne, J.L., Hand, M., Barovich, K.M., Reid, a., and Evans, D. a. D., 2009, Correlations and reconstruction models for the 2500-1500 Ma evolution of the Mawson Continent: Geological Society, London, Special Publications, v. 323, p. 319–355, doi: 10.1144/SP323.16.

Peacock, S.M., and Goodge, J.W., 1995, Eclogite-facies metamorphism preserved in tectonic blocks from a lower crustal shear zone , central Transantarctic Mountains , Antarctica: Lithos, v. 36, p. 1–13.

Peucat, J.J., Me, R.P., Monnier, O., and Fanning, C.M., 1999, Terre Adelie basement in the East-Antarctica Shield : geological and isotopic evidence for a major 1 . 7 Ga thermal event ; comparison with the Gawler Craton in South Australia: Precambrian Research, v. 94, p. 205–224.

Pisarevsky, S. a., Wingate, M.T.D., Li, Z.X., Wang, X.C., Tohver, E., and Kirkland, C.L., 2014, Age and paleomagnetism of the 1210Ma Gnowangerup-Fraser dyke swarm, Western Australia, and implications for late Mesoproterozoic paleogeography: Precambrian Research, v. 246, p. 1–15, doi: 10.1016/j.precamres.2014.02.011.

Powell, R., Holland, T., 1994, Optimal geothermometry and geobarometry: American Mineralogist, v. 79, p. 120–133.

Rignot, E; Mouginot, J.; Scheuchl, B., 2011, Ice flow of the Antarctic Ice Sheet: Science, v. 333, p. 1427–1430, doi: 10.1126/science.1208336.

Strickland, B.A., Wooden, J.L., Mattinson, C.G., Ushikubo, T., Miller, D.M., and Valley, J.W., 2013, Proterozoic evolution of the Mojave crustal province as preserved in the Ivanpah Mountains, southeastern California: Precambrian Research, v. 224, p. 222–241, doi: 10.1016/j.precamres.2012.09.006.

Van de Flierdt, T., Hemming, S.R., Goldstein, S.L., Gehrels, G.E., and Cox, S.E., 2008, Evidence against a young volcanic origin of the Gamburtsev Subglacial Mountains, Antarctica: Geophysical Research Letters, v. 35, p. L21303, doi: 10.1029/2008GL035564.

Whillans, I.M., and Cassidy, W.A., 1983, Catch a falling star: Meteorites and old ice: Science, v. 222, p. 55–57.

Will, T.M., Frimmel, H.E., Zeh, a., Le Roux, P., and Schmädicke, E., 2010, Geochemical and isotopic constraints on the tectonic and crustal evolution of the Shackleton Range, East Antarctica, and correlation with other Gondwana crustal segments: Precambrian Research, v. 180, p. 85–112, doi: 10.1016/j.precamres.2010.03.005.

Zeh, A., Millar, I. L., Horstwood, M.S.A., 2004, Polymetamorphism in the NE Shackleton Range, Antarctica: Constraints from Petrology and U-Pb, Sm-Nd, Rb-Sr TIMS and in situ U-Pb LA-PIMMS Dating: Journal of Petrology, v. 45, p. 949–973, doi: 10.1093/petrology/egg117.

Zhang, S., Li, Z.X., Evans, D. a D., Wu, H., Li, H., and Dong, J., 2012, Pre-Rodinia supercontinent Nuna shaping up: A global synthesis with new paleomagnetic results from North China: Earth and Planetary Science Letters, v. 353-354, p. 145–155, doi: 10.1016/j.epsl.2012.07.034.

Appendix A: Element maps of select garnets

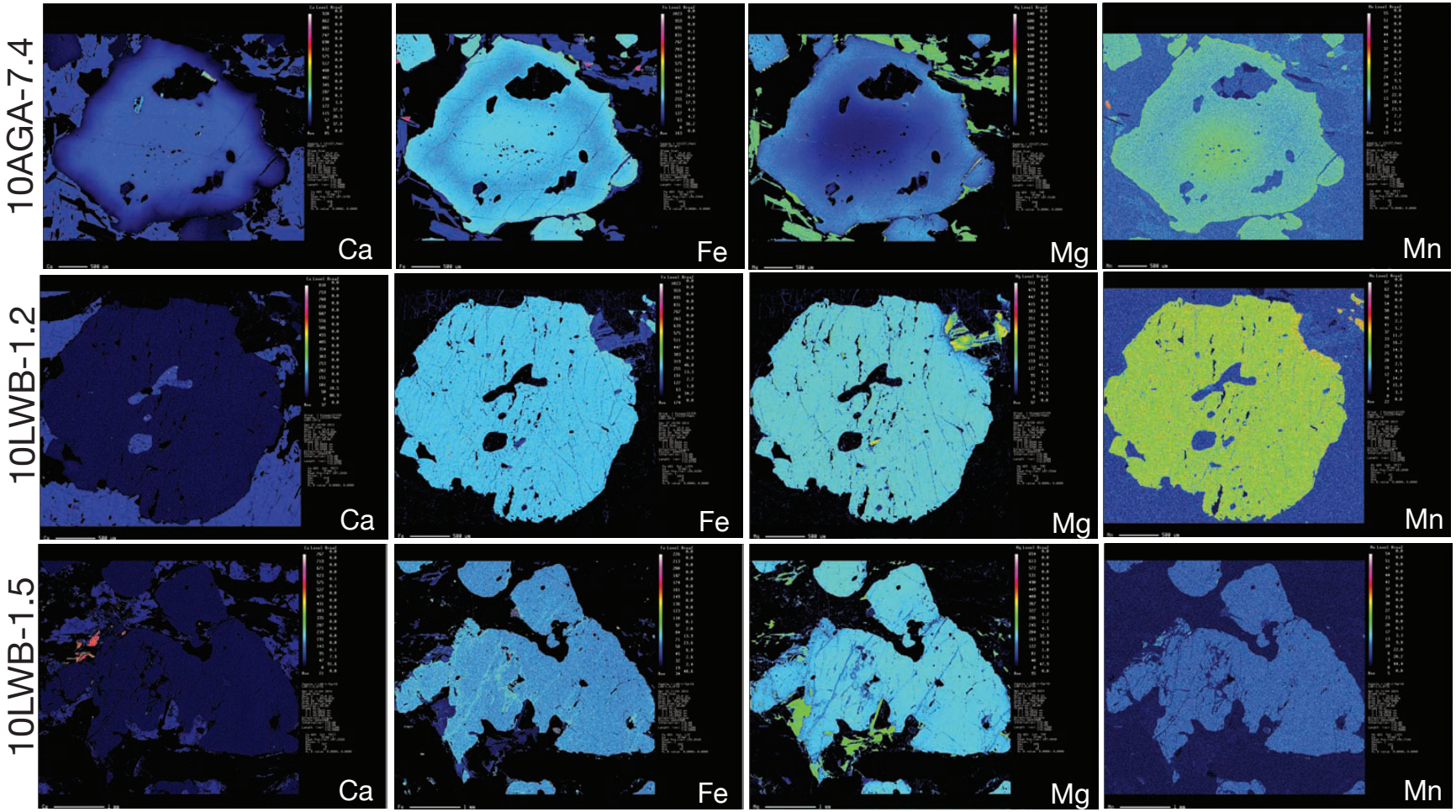

Element maps of garnets from samples 10AGA-7.4, 10LWB-1.2, and 10LWB-1.5. Garnet from sample 10AGA-7.4 shows elemental zoning in each component. Garnets from samples 10LWB-1.2 and 10LWB-1.5 do not show significant elemental zoning. Ca= calcium; Fe= iron; Mg= magnesium; Mn= manganese

Appendix B

Geothermobarometry

The mineral assemblage found in metamorphic rocks plays a key role in allowing geologists to determine the pressure-temperature (P-T) conditions of metamorphism they experienced. The mineral assemblage, in turn, is dependent upon the stability of the system, as expressed by thermodynamic properties. In thermodynamics, Gibbs Free Energy (G) expresses the total energy of a system as the sum of enthalpic and entropic energies. G is dependent on the internal energy of a phase (U), pressure (P), volume (V), temperature (T) and entropy (S). The relationship between these variables can be expressed by equation 1:

$$G = U + PV - TS \quad \textit{Equation 1}$$

The change in Gibbs free energy describes the energy the phase gains from not being able to expand minus the entropic energy (Equation 2):

$$\Delta G = \Delta H + P\Delta V - T\Delta S \quad \textit{Equation 2}$$

where H is the enthalpy of a system. The change in free energy of a mineral system undergoing reaction determines whether the reaction will produce more products or reactants. Equation 3 explains this by:

$$\Delta_r G = G_{products} - G_{reactants} \quad \textit{Equation 3}$$

Where $\Delta_r G$ is the change in Gibbs energy for the reactions (r). If $\Delta_r G$ is positive, the reaction will produce more reactants because extra energy is needed for the reaction to proceed. If $\Delta_r G$ is negative, there is enough energy in the system to produce products spontaneously (without help). When $\Delta_r G = 0$, the system is at

equilibrium and is stable; all natural systems work toward equilibrium, and thus, the lowest possible ΔG.

In thermobarometry, the changes in Gibbs free energy are produced by changes in pressure and temperature, which act on volume and entropy (respectively). However, these equations describe systems with ideal mixtures and most minerals are not ideal. Therefore, the activity () of a mineral must be specified. Activity is the effective concentration of a species in a mixture (e.g. elements in a mineral) and is a measure of how reactive a particular component will be. Activity is found by multiplying the activity coefficient by the mole fraction of a particular component to the power of their number in the general formula (Equation 4). For example, the generic formula for garnet is $X_3Al_2(SiO_4)_3$. Occupation of the 8-fold site, "X", varies chiefly between Mg, Fe^{2+}, Mn and Ca, making up the four main end-members of the garnet group: pyrope, almandine, spessartine and grossular, respectively. As diffusion occurs, substitution (individual or coupled), on the 8-fold site can only occur if charge and size of substituting element(s) are similar. If the mineral were an ideal end-member (example: 100% pyrope) the activity coefficient would be 1. However, garnet is rarely ideal, thus all end-member components present must be accounted for when calculating the activity (i.e. pyrope component).For garnet, each end-member component is accounted for using equation 4 for each of the elemental components, for a total of four separate equations (Mg, Ca, Fe^{2+}, and Mn). Conversely, quart and rutile are generally ideal in that their composition tends not to vary (SiO_2 and TiO_2, respectively).

The ratio of $_{products}/_{reactants}$ is known as the equilibrium constant (K_{eq}). By introducing the equilibrium constant into the Gibbs free energy equation, changes in composition of non-ideal phases are accounted for (Equation 4):

$$0 = \Delta G^{\circ}_{P,T} + RT\ln K \quad \text{Equation 4}$$

where R is the gas constant.

One approach to thermometry is the application of exchange reactions between minerals at varying pressure and temperature conditions; for example, the exchange of Fe^{2+} and Mg in garnet and clinopyroxene (Equations 5a and 5b) is controlled by diffusion and therefore T-dependent:

pyrope + 3 hedenbergite = almandine + 3 diopside Equation 5a

$$Mg_3Al_2(SiO_4)_3 + 3CaFeSi_2O_6 = Fe_3Al_2(SiO_4)_3 + 3\,MgCaSi_2O_6 \quad \text{Equation 5b}$$

This exchange has no major effect on volume (rather, on entropy) and therefore is more temperature sensitive. This reaction is represented by a steep slope on a P-T graph.

Conversely, barometry involves net-transfer reactions, which are pressure sensitive reactions indicating overall volume change. Net-transfer reactions produce new minerals as a result of a complete transfer of elements from one mineral to another; for example, the eclogite-facies bounding reaction involves a net transfer of elements from amphibole and plagioclase to form garnet + pyroxene (Equation 6a and 6b).

3 garnet + 2 pyroxene + water + 3 quartz = 2 amphibole + plagioclase Equation 6a

$$3Ca(Mg,Fe)_2Al_2(SiO_4)_3 + 2Ca(Mg,Fe)(SiO_3)_2 + 2H_2O + 3SiO_2 = 2Ca_2(Mg,Fe)_4Al_2Si_7O_{22}(OH)_2 + CaAl_2(SiO_4)_2 \quad \text{Equation 6b}$$

These reactions are dependent on the Clapeyron Equation (equation 7), which states that the slope of a reaction (dP/dT) is equal to the change in entropy (disorder) over the change in volume (ΔS/ΔV).

$$dP/dT = \Delta S/\Delta V \quad \text{Equation 7}$$

Thus, the shallower the slope, the more volume change; likewise, the steeper the slope, the less volume change. So, in P-T space, equilibria used as thermometers are expressed as steep lines, whereas equilibria used as barometer have low slope (Figure 2).

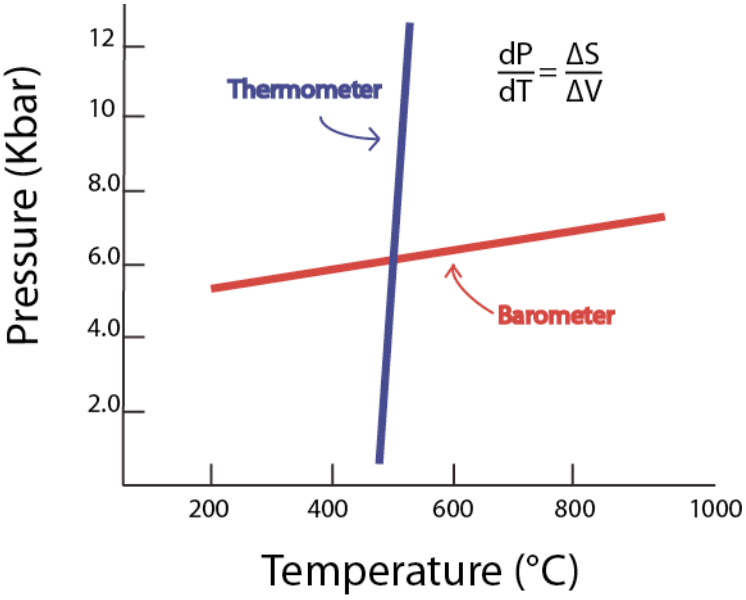

Figure 1: P-T diagram showing an example of a thermometer and barometer reaction line; in this example, two reactions in equilibrium yield a P-T estimate of ~6 kbar at 550 °C.

Calculating P-T Conditions

THERMOCALC (Powell & Holland, 1988, 1994) is a computer program that combines all of the thermodynamic variables involved in reaction to accurately estimate P and T of a specific mineral assemblage in a sample. This program uses element oxide data as input to calculate multiple mineral reactions. P-T estimates are derived through the optimization of end-member mineral reactions within a given pressure and temperature range using average P-T analysis. The simplest P-T calculations use single end-member reactions for equilibrium conditions (i.e., Grt-Bt thermometer), whereas the average P-T calculation in THERMOCALC utilizes multiple independent mineral equilibria within a given system using their internally consistent database. The system then becomes over-determined (meaning there are more reactions than unknowns) and an average P and T estimate is derived using the least-squares method (see Holland and Powell, 1994 for further discussion). These calculations include calculated mineral activities and associated uncertainties and correlations. Using multiple independent reactions and their uncertainties gives a more robust P-T estimate compared to single equilibrium reactions. Varying water content did not affect any of the calculations; thus water activity was assumed to be equal to 1.

Monazites

Metamorphic samples with an ideal mineral assemblage conducive to P-T analysis coupled with the presence of monazite are of particular interest due to the ability to radiometrically date monazites. Thus it is possible to associate age

with physical conditions of metamorphic reactions. Monazites are found in metamorphic rock samples from a number of glacial deposits in the central TAM. Monazite is a phosphate mineral ((Ca, La)PO_4) that incorporates trace and light rare-earth elements (La-Ce) and is stable at most metamorphic grades at and above the greenschist facies (Spear & Pyle, 2002). Monazite is an ideal candidate for U-Pb geochronology because it has low initial Pb concentrations but high Pb retention, as well as high U and Th contents (Kohn et al., 2005). Diffusion of trace elements in metamorphic minerals is slower than major elements, making monazite an ideal candidate for petrogenetic study. Similar to zircon, monazite may retain chemical zonation that can be used to provide ages for discrete events. Monazite is a metamorphic mineral and, when coupled with garnet-bearing metamorphic assemblages, it can be used to directly date a reaction and its position on a P-T-t path, thus giving a more thorough understanding of a rock's history (Williams & Jercinovic, 2012).

In some cases, Pb loss and inheritance in zircon can hinder its reliability for U-Pb dating, and while monazite is not without its complications, the use of both zircon and monazite allows for more robust radiometric chronology. In-situ U-Pb age dating of monazite, coupled with its textural setting, can lead to a better understanding of crustal growth and evolution.

Appendix C1: Summary of SHRIMP U-Pb results for monazite from sample AGA-7.2

Grain. spot	U (ppm)	Th (ppm)	Th/U	$^{206}Pb^*$ (ppm)	$^{204}Pb/^{206}Pb$	f_{206} %	Total $^{238}U/^{206}Pb$	±	Total $^{207}Pb/^{206}Pb$	±	Radiogenic $^{206}Pb/^{238}U$	±	Age (Ma) $^{206}Pb/^{238}U$	±	Age (Ma) $^{207}Pb/^{206}Pb$	±
2.1	1723	45,225	26.2	130.6	0.000074	<0.01	11.337	0.127	0.0584	0.0003	0.0882	0.0010	544.9	6.0	545	±13
4.1	*1962*	*997,659*	*508.5*	*268.7*	*0.008805*	*14.07*	*6.274*	*0.080*	*0.1833*	*0.0015*	*0.1370*	*0.0019*	*827.5*	*10.6*		
6.1	839	42,213	50.3	65.6	0.000176	<0.01	10.975	0.134	0.0585	0.0005	0.0912	0.0011	562.4	6.7	548	±17
6.2	548	38,379	70.0	44.3	0.000322	<0.01	10.625	0.143	0.0585	0.0006	0.0942	0.0013	580.4	7.6	549	±21
3A.1	849	26,543	31.3	64.3	0.000155	<0.01	11.345	0.149	0.0582	0.0005	0.0882	0.0012	544.7	7.0	536	±21

Notes: 1. Uncertainties given at the one σ level.

2. Error in 44069 reference monazite calibration was 0.65% for the analytical session.
(not included in above errors but required when comparing data from different mounts).

3. f_{206} % denotes the percentage of ^{206}Pb that is common Pb.

4. Correction for common Pb for the U/Pb data has been made using the measured $^{238}U/^{206}Pb$ and $^{207}Pb/^{206}Pb$ ratios following Tera and Wasserburg (1972) as outlined in Williams (1998).

Appendix C2: Summary of SHRIMP U-Pb results for monazite from sample AGA-7.4

Grain. spot	U (ppm)	Th (ppm)	Th/U	$^{206}Pb^*$ (ppm)	$^{204}Pb/^{206}Pb$	f_{206} %	Total $^{238}U/^{206}Pb$	±	Total $^{207}Pb/^{206}Pb$	±	Radiogenic $^{206}Pb/^{238}U$	±	Age (Ma) $^{206}Pb/^{238}U$	±
6.1	1212	47,846	39.5	93.6	0.000108	0.06	11.12	0.13	0.0592	0.0005	0.0898	0.0011	554.6	6.5
6.2	1241	45,686	36.8	94.0	0.000132	0.04	11.34	0.18	0.0587	0.0004	0.0881	0.0014	544.4	8.3
9.1	1389	68,067	49.0	109.7	0.000176	<0.01	10.88	0.13	0.0586	0.0004	0.0919	0.0011	567.0	6.4
8.1	556	41,054	73.8	42.5	0.000290	0.06	11.24	0.15	0.0590	0.0006	0.0890	0.0012	549.3	7.3
4.1	1137	50,260	44.2	85.2	0.000115	0.02	11.46	0.13	0.0584	0.0004	0.0872	0.0010	539.0	6.1

Notes: 1. Uncertainties given at the one σ level.

2. Error in 44069 reference monazite calibration was 1.56% for the analytical session.
(not included in above errors but required when comparing data from different mounts).

3. f_{206} % denotes the percentage of ^{206}Pb that is common Pb.

4. Correction for common Pb for the U/Pb data has been made using the measured $^{238}U/^{206}Pb$ and $^{207}Pb/^{206}Pb$ ratios following Tera and Wasserburg (1972) as outlined in Williams (1998).

	Age	± internal		**± include std: ie external**	
wtd ave dominant	**546.7**	6.8	2.00	**10.9**	MSWD =1.09 for 4 of 5 areas analysed

Appendix C3: Summary of SHRIMP U-Pb results for monazite from sample AGA-6.1

Grain. spot	U (ppm)	Th (ppm)	Th/U	$^{206}Pb^*$ (ppm)	$^{204}Pb/^{206}Pb$	f_{206} %	Total $^{238}U/^{206}Pb$	±	Total $^{207}Pb/^{206}Pb$	±	Radiogenic $^{206}Pb/^{238}U$	±	Age (Ma) $^{206}Pb/^{238}U$	±
8.1	2235	60,225	26.9	173.1	0.000053	0.06	11.09	0.12	0.0592	0.0003	0.0901	0.0010	556.1	6.1
7.1	2033	42,793	21.0	162.4	0.000088	<0.01	10.76	0.15	0.0587	0.0003	0.0930	0.0013	573.3	7.9
6.1	966	56,288	58.3	74.5	0.000173	0.10	11.15	0.14	0.0595	0.0007	0.0896	0.0012	553.4	6.8

Notes: 1. Uncertainties given at the one σ level.

2. Error in 44069 reference monazite calibration was 0.43% for the analytical session.

(not included in above errors but required when comparing data from different mounts).

3. f_{206} % denotes the percentage of ^{206}Pb that is common Pb.

4. Correction for common Pb for the U/Pb data has been made using the measured $^{238}U/^{206}Pb$ and $^{207}Pb/^{206}Pb$ ratios following Tera and Wasserburg (1972) as outlined in Williams (1998).

Appendix C4: Summary of SHRIMP U-Pb results for monazite from sample AGA-6.8

Grain. spot	U (ppm)	Th (ppm)	Th/U	$^{206}Pb^*$ (ppm)	$^{204}Pb/^{206}Pb$	f_{206} %	Total $^{238}U/^{206}Pb$	±	Total $^{207}Pb/^{206}Pb$	±	Radiogenic $^{206}Pb/^{238}U$	±	Age (Ma) $^{206}Pb/^{238}U$	±
9.1	1790	75,023	41.9	139.8	0.000253	0.10	11.00	0.14	0.0597	0.0006	0.0908	0.0012	560.6	6.9
9.2	2141	142,554	66.6	168.8	0.000098	<0.01	10.90	0.13	0.0586	0.0007	0.0918	0.0011	566.3	6.7
9.3	1057	43,887	41.5	80.8	0.000161	<0.01	11.24	0.13	0.0584	0.0005	0.0890	0.0010	~~549.7~~	~~6.2~~
10.1	1297	69,602	53.7	104.0	0.000098	<0.01	10.71	0.12	0.0589	0.0004	0.0934	0.0011	575.6	6.4
10.2	1437	79,879	55.6	109.6	0.000134	0.12	11.27	0.13	0.0595	0.0005	0.0886	0.0010	~~547.5~~	~~6.0~~
10.3	1166	52,607	45.1	92.0	0.000170	<0.01	10.88	0.12	0.0587	0.0004	0.0919	0.0011	566.9	6.3
10.4	1414	77,146	54.6	113.0	0.000138	<0.01	10.75	0.12	0.0587	0.0004	0.0931	0.0011	573.8	6.4
10.5	1372	60,511	44.1	107.5	0.000122	0.02	10.97	0.12	0.0590	0.0004	0.0912	0.0010	562.3	6.1
11.1	1588	82,942	52.2	126.6	0.000346	0.22	10.77	0.12	0.0609	0.0004	0.0926	0.0011	571.2	6.3
11.2	1222	62,145	50.9	97.2	0.000159	<0.01	10.80	0.12	0.0588	0.0004	0.0926	0.0011	571.1	6.4
11.3	1353	66,005	48.8	107.4	0.000140	<0.01	10.82	0.12	0.0589	0.0004	0.0924	0.0011	569.9	6.2
12.1	1108	53,130	47.9	89.2	0.000123	<0.01	10.67	0.12	0.0583	0.0004	0.0938	0.0011	578.2	6.4
12.2	1259	60,559	48.1	96.8	0.000126	0.05	11.18	0.12	0.0590	0.0004	0.0894	0.0010	~~552.1~~	~~6.0~~
12.3	1588	82,385	51.9	125.5	0.000456	0.54	10.87	0.12	0.0633	0.0005	0.0915	0.0010	564.5	6.1

Notes: 1. Uncertainties given at the one σ level.

2. Error in 44069 reference monazite calibration was 0.43% for the analytical session.

(not included in above errors but required when comparing data from different mounts).

3. f_{206} % denotes the percentage of ^{206}Pb that is common Pb.

4. Correction for common Pb for the U/Pb data has been made using the measured $^{238}U/^{206}Pb$ and $^{207}Pb/^{206}Pb$ ratios following Tera and Wasserburg (1972) as outlined in Williams (1998).

	Age	± internal		**± include std: ie external**	
wtd ave dominant	**569.1**	3.8	0.79	**4.5**	MSWD = 0.74 for 11 of 14 areas analysed

Appendix C5: Summary of SHRIMP U-Pb results for monazite from sample MRA-11.3

Grain. spot	U (ppm)	Th (ppm)	Th/U	$^{206}Pb^*$ (ppm)	$^{204}Pb/^{206}Pb$	f_{206} %	Total $^{238}U/^{206}Pb$	±	Total $^{207}Pb/^{206}Pb$	±	Radiogenic $^{206}Pb/^{238}U$	±	Age (Ma) $^{206}Pb/^{238}U$	±
1.1	468	21,817	46.6	38.6	0.000142	0.05	10.428	0.131	0.0601	0.0005	0.0958	0.0012	590.0	7.2
1.2	603	7,294	12.1	49.5	0.000106	<0.01	10.471	0.126	0.0589	0.0005	0.0956	0.0012	588.4	6.9
2.1	463	67,176	145.1	38.3	0.002172	3.10	10.384	0.155	0.0845	0.0010	0.0933	0.0014	575.1	8.4
3.1	467	46,631	99.9	38.2	0.000360	0.09	10.496	0.150	0.0602	0.0008	0.0952	0.0014	586.2	8.2
5.1	2721	54,380	20.0	251.1	0.001007	1.66	9.311	0.100	0.0748	0.0003	0.1056	0.0012	647.2	6.7
5.2	2402	65,196	27.1	221.3	0.000242	0.32	9.324	0.101	0.0641	0.0007	0.1069	0.0012	654.7	6.9
6.1	2065	55,461	26.9	191.3	0.000055	0.10	9.274	0.100	0.0624	0.0002	0.1077	0.0012	659.6	6.9
6.2	1744	42,092	24.1	164.4	0.000068	0.09	9.114	0.106	0.0627	0.0003	0.1096	0.0013	670.5	7.6
7.1	544	12,658	23.3	45.2	0.000151	0.03	10.354	0.128	0.0600	0.0005	0.0966	0.0012	594.2	7.2
8.1	417	29,611	70.9	35.7	0.000291	<0.01	10.033	0.136	0.0600	0.0006	0.0997	0.0014	612.7	8.1
8.2	1620	47,718	29.5	135.4	0.000116	0.06	10.277	0.115	0.0604	0.0003	0.0972	0.0011	598.3	6.5
10.1	364	21,217	58.3	31.5	0.000214	<0.01	9.932	0.131	0.0596	0.0005	0.1008	0.0014	619.0	7.9
10.2	456	13,924	30.5	38.3	0.000087	<0.01	10.223	0.129	0.0599	0.0005	0.0978	0.0013	601.6	7.4

Notes: 1. Uncertainties given at the one σ level.

2. Error in 44069 reference monazite calibration was 0.43% for the analytical session.
(not included in above errors but required when comparing data from different mounts).

3. f_{206} % denotes the percentage of ^{206}Pb that is common Pb.

4. Correction for common Pb for the U/Pb data has been made using the measured $^{238}U/^{206}Pb$ and $^{207}Pb/^{206}Pb$ ratios following Tera and Wasserburg (1972) as outlined in Williams (1998).

	Age	± internal		**± include std: ie external**	
wtd ave main grouping	**593.4**	5.7	1.05	**6.2**	MSWD = 0.66 for 6 of 13 areas analysed

Appendix C6: Summary of SHRIMP U-Pb monazite results for sample LWB-1.2

Grain. spot	U (ppm)	Th (ppm)	Th/U	$^{206}Pb^*$ (ppm)	$^{204}Pb/^{206}Pb$	f_{206} %	Total Ratios $^{238}U/^{206}Pb$	±	$^{207}Pb/^{206}Pb$	±	Radiogenic Ratios $^{207}Pb/^{235}U$	±	$^{206}Pb/^{238}U$	±	ρ	$^{207}Pb/^{206}Pb$	±	Age (Ma) $^{206}Pb/^{238}U$	±	$^{207}Pb/^{206}Pb$	±	% Disc
4.1	*205*	*625*	*3.0*	*38.2*	*0.000093*	*<0.01*	*4.616*	*0.074*	*0.0693*	*0.0008*	*2.026*	*0.042*	*0.2163*	*0.0035*	*0.773*	*0.0679*	*0.0009*	*1262*	*18*	*866*	*27*	*-46*
4.2	*215*	*704*	*3.3*	*42.6*	*0.000032*	*<0.01*	*4.340*	*0.072*	*0.0689*	*0.0008*	*2.174*	*0.046*	*0.2303*	*0.0038*	*0.786*	*0.0685*	*0.0009*	*1336*	*20*	*883*	*27*	*-51*
6.1	*108*	*4,046*	*37.5*	*23.8*	*0.001509*	*<0.01*	*3.892*	*0.072*	*0.0804*	*0.0017*	*2.026*	*0.121*	*0.2507*	*0.0047*	*0.314*	*0.0586*	*0.0033*	*1442*	*24*	*553*	*124*	*-161*
5.1	1867	37,383	20.0	462.2	0.000061	0.57	3.470	0.057	0.1049	0.0002	4.132	0.069	0.2879	0.0048	0.986	0.1041	0.0003	1631	24	1698	5	4
5.2	2751	51,339	18.7	697.7	0.000040	0.20	3.388	0.053	0.1040	0.0004	4.206	0.067	0.2950	0.0046	0.969	0.1034	0.0004	1666	23	1686	7	1
3.2	2792	49,462	17.7	733.3	0.000023	0.59	3.271	0.036	0.1099	0.0002	4.616	0.052	0.3056	0.0033	0.979	0.1096	0.0002	1719	17	1792	4	4
3.3	3277	58,658	17.9	952.8	0.000063	0.01	2.955	0.032	0.1150	0.0002	5.322	0.059	0.3381	0.0037	0.979	0.1142	0.0003	1877	18	1867	4	-1
2.1	544	53,562	98.5	160.4	0.000349	0.20	2.911	0.037	0.1180	0.0007	5.337	0.088	0.3416	0.0044	0.782	0.1133	0.0012	1895	21	1853	19	-2
3.1	2280	43,671	19.2	679.3	0.000022	<0.01	2.883	0.036	0.1147	0.0002	5.468	0.069	0.3467	0.0043	0.985	0.1144	0.0003	1919	21	1870	4	-3

Notes :

1. Uncertainties given at the one σ level.
2. Error in 44069 reference monazite calibration was 0.43% for the analytical session.
   (not included in above errors but required when comparing $^{206}Pb/^{238}U$ data from different mounts).
3. f_{206} % denotes the percentage of ^{206}Pb that is common Pb.
4. Correction for common Pb made using the measured $^{204}Pb/^{206}Pb$ ratio.
5. For % Disc, 0% denotes a concordant analysis.

Appendix C7: Summary of SHRIMP U-Pb monazite results for sample LWB-1.5

Grain. spot	U (ppm)	Th (ppm)	Th/U	$^{206}Pb^*$ (ppm)	$^{204}Pb/^{206}Pb$	f_{206} %	Total Ratios				Radiogenic Ratios				ρ	Age (Ma)						% Disc
							$^{238}U/^{206}Pb$	±	$^{207}Pb/^{206}Pb$	±	$^{207}Pb/^{235}U$	±	$^{206}Pb/^{238}U$	±		$^{207}Pb/^{206}Pb$	±	$^{206}Pb/^{238}U$	±	$^{207}Pb/^{206}Pb$	±	
5.1	68	11,896	174.4	11.2	0.002741	4.89	5.214	0.153	0.0984	0.0021	1.472	0.171	0.1824	0.0055	0.260	0.0585	0.0065	1080	30	549	244	-97
3.1	642	30,777	48.0	110.4	0.000400	0.67	4.994	0.063	0.0827	0.0010	2.112	0.044	0.1989	0.0025	0.618	0.0770	0.0012	1169	14	1122	32	-4
5.2	747	28,189	37.7	130.5	0.000557	0.93	4.919	0.064	0.0867	0.0006	2.189	0.044	0.2014	0.0026	0.642	0.0788	0.0012	1183	14	1168	31	-1
1.1	652	33,710	51.7	116.1	0.000805	1.36	4.826	0.062	0.0870	0.0005	2.130	0.041	0.2044	0.0026	0.669	0.0756	0.0011	1199	14	1084	29	-11
2.1	763	31,446	41.2	135.4	0.000113	0.19	4.843	0.060	0.0787	0.0004	2.190	0.031	0.2061	0.0025	0.868	0.0771	0.0005	1208	14	1123	14	-8
3.2	224	22,443	100.0	47.5	0.002166	3.52	4.055	0.076	0.1206	0.0010	2.967	0.118	0.2379	0.0045	0.480	0.0905	0.0031	1376	24	1435	66	4
4.1	1597	66,258	41.5	409.1	0.000092	0.14	3.353	0.038	0.1085	0.0007	4.403	0.057	0.2978	0.0033	0.867	0.1072	0.0007	1681	17	1753	12	4
4.2	667	97,008	145.4	181.6	0.000261	0.40	3.156	0.043	0.1155	0.0005	4.871	0.075	0.3156	0.0043	0.894	0.1119	0.0008	1768	21	1831	12	3

Notes :

1. Uncertainties given at the one σ level.
2. Error in 44069 reference monazite calibration was 0.65% for the analytical session.
   (not included in above errors but required when comparing $^{206}Pb/^{238}U$ data from different mounts).
3. f_{206} % denotes the percentage of ^{206}Pb that is common Pb.
4. Correction for common Pb made using the measured $^{204}Pb/^{206}Pb$ ratio.
5. For % Disc, 0% denotes a concordant analysis.